City and Environment Interactions 28 (2025) 100245

Contents lists available at ScienceDirect

City and Environment Interactions

journal homepage: www.sciencedirect.com/journal/city-and-environment-interactions

Research Articles

Analysing Surface Urban Heat Island risks: mapping the vulnerability of dwelling and dwellers across Swedish municipalities

Charafeddine Mokhtara [a,b], Shashwat Sinha [a], Ashmin Aryal [a,*], Brijesh Mainali [a], Krushna Mahapatra [a]

[a] Department of Built Environment and Energy Technology, Linnaeus University, Växjö, Sweden
[b] Department of Mechanical Engineering, Faculty of Technology, University of El Oued, El Oued, Algeria

ARTICLE INFO

Keywords:
Climate change
Urban heat island
Social vulnerability
Risk assessment
Geographic information system
Resilience

ABSTRACT

Sweden's average temperature has increased by 1.9 °C since the late 19th century and is projected to rise by another 3–5 °C by the end of the century. As urbanisation amplifies heat stress, there is an urgent need to assess Surface Urban Heat Island (SUHI) risks, especially in high-latitude regions like Sweden, where such studies are limited. This study maps SUHI hazards, exposure, and vulnerability across Sweden to identify high-risk municipalities, focusing on residents in Single-Family Houses (SFHs). MODIS-derived land surface temperature (LST) data (2015–2022) were used to estimate SUHI intensity (hazard). Population density and building footprint data informed exposure, while vulnerability was measured using a Composite Vulnerability Index (CVI) based on social and physical indicators, including population demographics and building-related characteristics. All indicators and risk components were normalised, weighted using entropy and PCA, and integrated through geospatial analysis to produce a 1 km resolution national SUHI risk map, validated using heat-related mortality data. Results indicate that high-risk areas are concentrated in major cities. 12 high-risk municipalities contain 14 % of all SFHs built before 1975, and 18 medium-risk municipalities contain 8 %, together accounting for 22 % of the national pre-1975 SFH stock. Residents of these SFHs represent nearly half of those living in pre-1975 SFHs nationwide. These findings highlight the urgent need for climate-smart renovations with strategies like reflective roofing, increased greenery, and soft financing for urban adaptation planning in northern climates.

Introduction

Urban expansion and population growth have increased atmospheric CO_2 levels from about 280 parts per million in pre-industrial times to around 410 parts per million today [1]. This rise has caused global temperatures to increase by 1.1 °C, with even higher warming over land. According to the IPCC Sixth Assessment Report, global temperatures could rise by 2.1 to 3.5 °C by the year 2100 if emissions are not reduced [1]. In more extreme scenarios, this warming could happen as early as 2041 to 2060. At the same time, more people are moving into cities. Currently, 57 per cent of the world's population lives in urban areas, and this is expected to grow to 68 per cent by 2050 [2]. The combined effect of climate change and rapid urban growth is expected to make the Urban Heat Island (UHI) problem worse. As a result, UHI has become an important issue that needs urgent attention.

UHI is a localised area within a city that is warmer than the surrounding rural areas [3,4]. UHIs are influenced by urban geometry, construction materials, and vegetation cover [5,6]. Factors such as building height, street width, built area ratio, and the size of open spaces affect how temperatures are distributed in cities [7].The high concentration of built structures with impervious surfaces, and lack of greenery, suppresses the evaporative cooling and changes the urban energy balance by increased absorption and heat storage due to the inherent high thermal mass [8]. The UHI effect exacerbates anthropogenic heat emissions [9], varying with spatial and temporal distribution [10]. UHI causes various negative impacts like decreased thermal comfort and higher energy usage in buildings [11,12]. UHI is divided into two categories: Atmospheric UHI and Surface Urban Heat Island (SUHI) [13]. When the air temperature on site is used to calculate the UHI, it is referred to as the atmospheric UHI. Atmospheric UHI, which includes the Canopy Layer Heat Island (CLHI) and Boundary Layer Heat Island (BLHI), is measured using in-situ instrumentation. These methods provide high temporal resolution and can capture vertical temperature profiles, but they are cost-intensive, logistically complex, and generally limited to large metropolitan areas with adequate infrastructure. The

* Corresponding author.
E-mail address: ashmin.aryal@lnu.se (A. Aryal).

https://doi.org/10.1016/j.cacint.2025.100245
Received 25 February 2025; Received in revised form 27 July 2025; Accepted 9 September 2025
Available online 14 September 2025
2590-2520/© 2025 The Author(s). Published by Elsevier Ltd. This is an open access article under the CC BY license (http://creativecommons.org/licenses/by/4.0/).

Nomenclature

List of abbreviations

CC	Climate Change
GIS	Geographical information system
LST	Land surface temperature
MODIS	Moderate Resolution Imaging Spectroradiometer
RCP	Representative Concentration Pathway
RS	Remote sensing
SCB	Statistics Sweden (Statistiska centralbyrån or SCB)
SE	Sweden
SFH	Single Family Houses
SSP	Socioeconomic Pathways
SUHI	Surface Urban Heat Island
UHI	Urban Heat Island
UN	United nation
USGS	The United States Geological Survey
AR	Assessment report
CCRM	Climate Change Risk Management

term SUHI is used when Land Surface Temperature (LST) data is considered. SUHI is strongly related to the heat-absorbing characteristics of surfaces and materials rather than atmospheric causes; its mechanisms are simpler than those of atmospheric UHI [14]. Atmospheric UHI measurements often lack the spatial coverage needed for fine-scale national climate adaptation planning. In contrast, SUHI is assessed using thermal remote sensing from satellites such as MODIS, Landsat, and Sentinel. These provide consistent and wide-area data at different spatial and temporal resolutions, allowing for multi-scale analysis of LST patterns [15]. Satellite-based LST data is now widely available, reliable, and commonly used in urban climate research.

The UHI effect is evident across the world, affecting built-up areas of all sizes, from small villages and towns to major cities where UHI intensity is most pronounced [16,17]. This widespread phenomenon influences human settlements globally, from remote Arctic locales like Barrow, Alaska, to bustling metropolises like New York City [18]. Sweden is also not immune to heat-related extremes. Despite its high-latitude location and perceived low vulnerability, the country faced a record-breaking heatwave in the last decade (2018 and 2023), with elevated heat-related mortality [19]. This event highlights Sweden's growing exposure to rising global temperatures, a trend expected to intensify in the coming decades.

Sweden is also not immune to heat-related extremes. Despite its high-latitude location and perceived low vulnerability, the country faced a record-breaking heatwave in the last decade (2018 and 2023), with elevated heat-related mortality [19]. This event highlights Sweden's growing exposure to rising global temperatures, a trend expected to intensify in the coming decades. A key factor that has shaped Sweden's contemporary urban landscape is the Million House Programme (1965–1975), a large initiative launched by the Swedish government to construct one million homes within a decade [20]. This ambitious program accelerated urbanisation by promoting internal migration from rural areas and supporting labour mobility through rapid housing expansion in urban and suburban regions [21]. As a result, a significant share of Sweden's current housing stock originates from this period: approximately one third of all existing Single-family houses (SFHs) were built during the Million House program [21]. SFHs in Sweden account for 43 % of Sweden's building stock and 40 % of residential energy consumption. Many of these homes are energy-inefficient, primarily house elderly residents, and require substantial renovations [22,23]. Given Sweden's building stock with a low energy renovation rate and the vulnerability of SFHs and their residents, this research is crucial for identifying priority areas for renovation to enhance energy efficiency and climate resilience, particularly in addressing SUHI risk. This type of research will help stakeholders comply with Ordinance 2018:1428, issued by the Swedish government, which highlights the importance of studying climate vulnerability across all Swedish municipalities [24].

This study aims to assess, map, and analyse the SUHI risk and vulnerability of different municipalities in Sweden, to strengthen the building sector's resilience. The main contributions of this work are (i) mapping SUHI intensity (hazard), exposure (of population and buildings), and vulnerability of SFH and its residents, (ii) mapping SUHI risk areas by combining hazard, exposure and vulnerability and (iii) identifying municipalities and cities in high-risk areas.

The novelty of this research lies in its national-scale SUHI risk mapping focused on SFHs in a high-latitude country, integrating open-source satellite remote sensing data with various physical and social vulnerability indicators.

State of the art of SUHI risk assessment and mapping

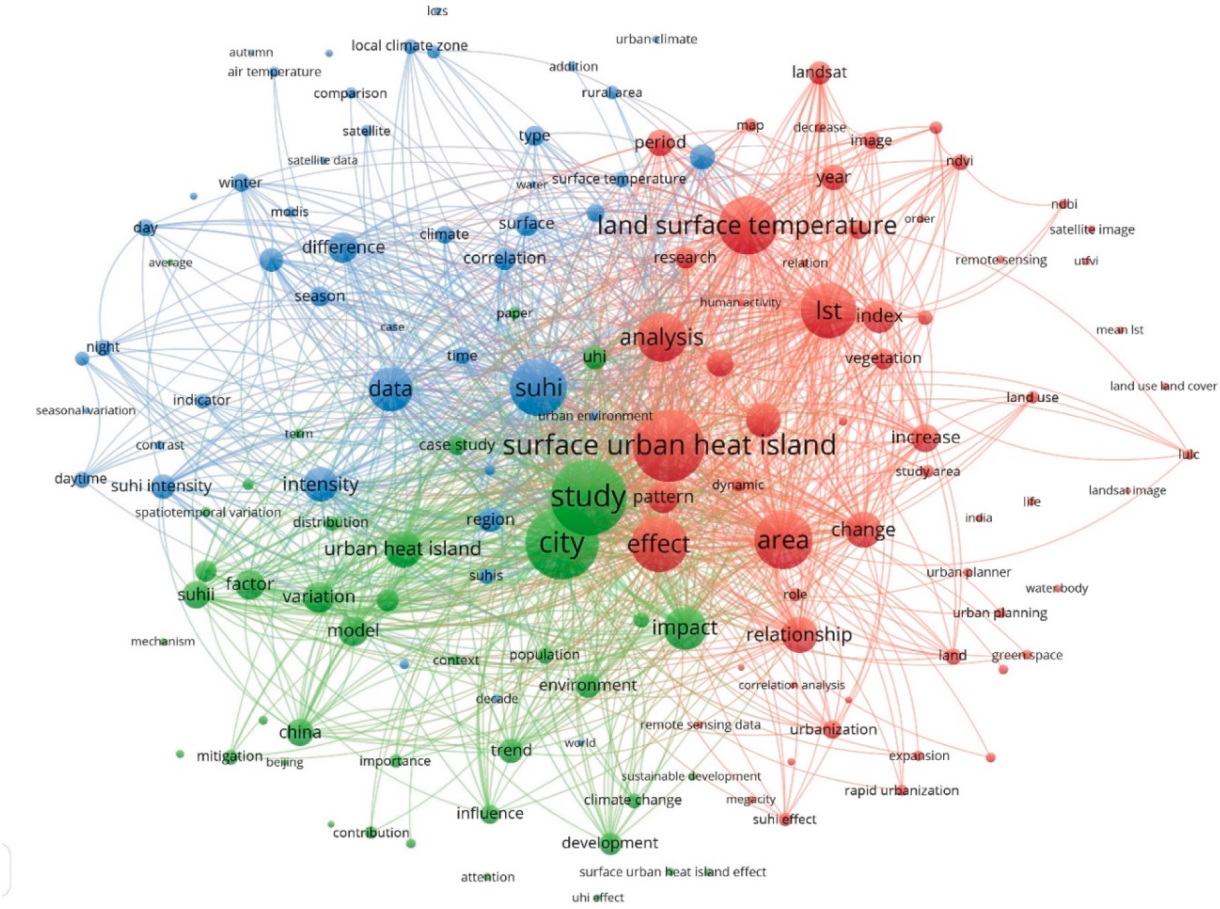
Bibliometric analysis was performed by searching relevant articles in the Scopus database. We searched for articles published between 2020 and 2024 that have "surface urban heat island" in their title, abstract, or keywords, along with the terms "assessment," "mapping," or "analysis." Only Journal articles in English were considered, resulting in 380 articles. The VOS viewer tool was used to identify and classify the main topics within the literature [25]. Fig. 1 illustrates the key themes and interconnections in SUHI research, visualised through a VOS viewer network based on bibliometric analysis of abstracts and titles retrieved from Scopus. A total of 276 terms with a minimum occurrence of 15 were analysed using a binary counting method. To ensure relevance, the top 60 % of the most pertinent terms were selected for inclusion in the visualisation. The network visualisation of SUHI research reveals three distinct thematic clusters. Within the network, term connections, shown by lines, show that terms frequently appear together in documents. Inter-cluster connections indicate multidisciplinary linkages, but dense connections within clusters emphasise themes that are closely related. Strongly linked nodes, such as "surface urban heat island," "study," "data," and "land surface temperature", serve as central terms linking multiple sub-themes. The three clusters from the bibliometric analysis are interpreted and described below:

Study the effects of SUHI and suggest mitigation strategies and policies

In response to environmental changes and the rise of SUHI intensity, a growing body of literature emphasises the importance of mitigation strategies aimed at enhancing urban thermal comfort and reducing SUHI intensity (as shown in cluster 1). Various strategies have been proposed to mitigate SUHI, including urban shading [26]and increasing green cover [27–29]. These include upgrading buildings with improved insulation, passive cooling measures (e.g., solar shading, reflective roofs, and natural ventilation), and renewable-integrated HVAC systems [30]. Nature-based solutions such as green roofs, green walls, and expanded urban vegetation cover play a central role in these strategies [14,31–34]. The role of vegetation in ameliorating the microclimate through evapotranspiration, shading, and cooling has been highlighted by various studies [35–37], indicating the critical need for green infrastructure in urban planning. These findings underscore the urgent need to prioritise strategies such as urban forests, green roofs, and sustainable land-use planning to enhance the urban microclimate and mitigate UHI effects.

Changes in environment and climate variables and their influence on or correlation with SUHI

Cluster 2 of the bibliometric analysis focuses on the relationship between environmental and climate variables and SUHI intensity. Key themes include changes in Land Use and Land Cover (LULC) variables



(a)

Cluster		Gaps
Cluster 1:	1-Data-driven methods for formulating adaptation and mitigation strategies. 2-Analysing nature-based mitigation strategies to ensure their ability to reduce the effects of SUHI.	A few case studies from high-latitude regions like Sweden
Cluster 2:	1-Study changes in urbanisation, human activities, land use (vegetation, water…), expansion of infrastructure, NDVI, NDBI. 2-Study correlation between factors (such as NDVI, urban morphology) and SUHI.	
Cluster 3:	Mapping SUHI in various cities in the USA, China, and Europe. etc, considering spatial and temporal variations.	-Few studies discuss the combined effects of SUHI on both population and infrastructure (buildings) at the country scale. -Limited work to perform comprehensive risk assessments needed for tailored and national-scale resilience planning.

(b)

Fig. 1. Bibliometric network visualisation of SUHI-related research topics. (a) the network structure derived from term co-occurrence analysis using VOSviewer, (b) thematic clusters' summary.

such as NDVI, NDBI, vegetation, urbanisation, and water bodies [38–40]. These studies show that urban expansion and LULC changes significantly influence land surface characteristics, which regulate SUHI formation through altered energy balance and heat fluxes [14,41,42]. Urban features like low-albedo materials, dense geometry, and anthropogenic heat further exacerbate SUHI intensity [5,6], while meteorological elements such as solar radiation, humidity, wind speed, and proximity to water bodies also play key roles [43–47]. The literature also reveals strong associations between SUHI and factors like city size, built-up area, and population density [28,48–51], though findings vary by context [52]. Urban morphology, particularly 2D characteristics and the height-to-width (H/W) ratio of buildings, is shown to influence LST [53–57], while the complexity of urban form, including fractality and anisometry, affects UHI patterns [58]. The sky view factor, building height, typology, and materials significantly impact microclimates [59–62].Machine learning is increasingly used to capture complex, nonlinear relationships among these variables and improve SUHI prediction accuracy [63]. Additionally, studies have explored how climate change interacts with SUHI, with findings showing that rising temperatures, reduced wind speed and cloud cover, and increased anthropogenic heat elevate SUHI impacts and urban cooling demands [64–69].

SUHI intensity mapping

Cluster 3 includes studies that map SUHI intensity using satellite-derived Land Surface Temperature (LST) data from sources like MODIS, Landsat, and Sentinel. These studies focus on city-scale to national-level analyses, supporting urban policy and risk assessment. The integration of Earth observation data with socio-economic and urban structural datasets enhances the precision and applicability of SUHI mapping. These tools are shown to aid climate adaptation and urban planning by offering data-driven insights for developing heat-resilient cities. Notably, their limited application in Nordic countries points to a key area for future research. Table 1 summarises key studies addressing UHI intensity (hazard) at broader spatial scales, reinforcing the relevance of large-scale analyses in supporting urban climate adaptation efforts.

According to the above literature, it is observed that UHI is mostly affected by the change in climate attributes (mainly LST), LULC (like forest area, vegetation, water bodies), and urbanisation (such as building density, and infrastructure development). Most previous studies used Geographical Information System (GIS) and Remote Sensing (RS) tools to assess and map UHI hazards, vulnerability, and risk, primarily at the city level and in high-temperate regions. These studies also highlighted the role of data-driven methods such as big data and machine learning, as well as the integration of various data sources, such as socio-economic records with remote sensing and meteorological data, enabling large-scale, dynamic assessments and multifactorial analyses of SUHI and formulating climate adaptation strategies. Although the stated studies provide useful information, there is still a need for assessing and mapping the SUHI risk for multi-cities at the country level, specifically in high-latitude regions like Sweden, to guide authorities in establishing national adaptation and mitigation policies for UHI risk and provide useful information to all householders. Additionally, identifying municipalities in high-risk areas is crucial for assisting policymakers and homeowners in making informed decisions regarding mitigation and adaptation to counteract the adverse effects of SUHI. Furthermore, developing a comprehensive assessment method based on open-source data and tools, which is easily replicable, can help in advancing Climate Change Risk Management (CCRM) globally. Thus, more comprehensive studies are crucial to overcome the shortcomings in the literature and provide more tailored mitigation strategies which could get high acceptance from all stakeholders at the case study location.

This study leverages these advanced spatial datasets and analytical techniques to provide detailed insights into SUHI patterns, which are essential for effective urban CCRM. Given the limited application of such comprehensive approaches in Nordic contexts, this research fills an important gap by adapting and applying these methodologies to a region (mainly Sweden) where urban heat challenges are emerging but less studied, thereby contributing valuable knowledge for local climate adaptation and resilient urban planning.

Methods and data

The conceptual framework for assessing SUHI risk in Sweden is presented in Fig. 2. This framework is adapted from the standard risk assessment frameworks provided in the IPCC assessment report AR5 [82]. The developed framework is an interplay among exposure, climate-related hazards, and vulnerability. Hazards are potential unfavourable occurrences that might affect life, livelihood, infrastructure, the supply of services, and environmental resources. In this study, the term “hazard” refers to the increased intensity of the SUHI. “Exposure” is defined as the existence of components in locations that may be negatively impacted by occurrences and are therefore prone to possible harm, loss, or damage; the exposure is the human population and houses in this study. “Vulnerability” denotes the circumstances influenced by physical, social, economic, and environmental elements or processes that elevate the sensitivity of individuals, communities, assets, or

Table 1
SUHI studies at the multicity level and the national level.

Country	Data source	Findings	SUHI Values
Brazil [70]	Terra	Nighttime UHI is influenced by urban density and building materials, and daytime by urban form and vegetation.	São Paulo and Rio de Janeiro showed daily UHI values above 1.5 ∘C, and nighttime UHI above 2.5 ∘C
Canada [71]	Aqua	City size, elevation, and surrounding land cover shape SUHI characteristics	SUHI magnitude range (−3 to 6.1 K)
China [72]	–	Reducing the building density and height mitigates UHI. UHI effect varies under different regional climatic conditions.	An average annual UHI of 1–2.3 °C
China [10]	Aqua, Landsat TM/ETM, DMSP/OLS	SUHII varies by region, time, and season, higher in summer days, and winter nights are influenced by vegetation, heat releases and climate.	The annual mean SUHI varied markedly from 0.01 to 1.87 °C in the day and 0.35 to 1.95 °C at night, with a great deal of spatial heterogeneity
China [73]	Terra, Aqua, NOAA-11, DMSP/OLS	Climate, land use, topography, and vegetation coverage affect SUHI in cities. Positive correlation with GDP, population, electricity bills, and built-up area	Highest mean SUHI of 4.3 K
European Cities [74]	Terra	Urban density is a key factor in SUHI spatial variability; higher LSTs occur in denser city areas. LST varies by location.	Urban and industrial areas have significantly higher LSTs (4–6 °C) than green urban areas and agricultural areas within cities.
European cities [75]		UHI intensifies during heatwaves in most European cities.	Mean SUHI −3.8–3.8∘C
India [76]	Terra, Aqua, DMSP/OLS	Impacted by anthropogenic activities.	Intense SUHII in tropical day (Chennai and Kolkata (1.21 °C and 1.33 °C)) and arid/temperate night (Delhi and Ahmedabad (2.25 °C and 2.23 °C))
Italy [77]	Terra	Impervious surface and tree cover influence SUHI. Coastal cities have less intense SUHI	Max 8.4 LST difference
Romania [78]	Terra, Aqua	UHI is influenced by population, area size, climate type and LULC	Nighttime SUHII is around 0.9 ∘C in summer months, daytime SUHII varies from 1.9 ∘C-2.5 ∘C
Fennoscandia [79]	Terra	Intense SUHI in coastal cities of the Atlantic region. Cities with warmer rural backgrounds have lower SUHI intensity, and colder rural climates have higher SUHI intensity (3–5 °C).	Mean SUHI range 0-5∘C
USA [80]	Terra, Aqua, DMSP/OLS	Annual Temperature Cycle (ATC) in urban/rural areas influenced	Max mean SUHI value of 4.8 K

(*continued on next page*)

Table 1 (*continued*)

Country	Data source	Findings	SUHI Values
		by urban land cover/ urbanisation.	
USA[81]	AQUA, LANDSAT/ ETM + IKONOS	Ecological context influences summer daytime UHI. The largest UHI amplitude was observed in temperate broadleaf and mixed forest biomes. UHI amplitude increases with city size and is seasonally asymmetric.	The largest summertime daytime UHI amplitude is 8 °C. Average UHI amplitude: 4.3 °C in summer and 1.3 °C in winter.

systems to the effects of hazards; in this study the low energy performance and aged Single-family houses and their vulnerable residences that are likely to be affected by SUHI intensity (hazard) are considered.

As illustrated in the conceptual framework, the SUHI intensity map is assessed based on Land Surface Temperature (LST) from MODIS data. After that, exposure is evaluated by merging building and population density maps produced based on Open Street Maps (OSM) data and geodata from SCB for Swedish localities. Vulnerability is assessed by analysing the sensitivity and adaptive capability of Single-Family Homes (SFH) and their inhabitants, through the development of a Composite Vulnerability Index (CVI) that combines a Population Social Vulnerability Index (PSVI) and a Buildings Physical Vulnerability Index (BPVI).

Integration of these maps assists in the identification of high-risk areas and identifies vulnerable elements in municipalities and cities at high risk, enabling effective adaptation and mitigation planning and reducing SUHI effects in Sweden. This study will guide policymakers and stakeholders in implementing targeted interventions and emergency response preparation to reduce vulnerability and increase the resilience of buildings and people located in risky areas, as well as transfer knowledge and lessons learned for other countries.

Location description

Sweden lies between latitudes 55° N and 69° N and longitudes 11° E and 23° E. Its overall surface area is 528,447 km^2, with a land area of 408,150 km^2 [19]. As per the Köppen-Geiger climate classes, the climate of Sweden is classified into three climate zones: climate zone 1: cold humid cold summers (Dfc), climate zone 2: cold humid warm summers (Dfb) and climate zone 3: temperate humid warm summers (Cfb) [84]. Fig. 3 shows the map of Sweden, containing its counties (21 counties) and municipalities (290 municipalities).

Satellite data

Satellite plays a significant role in providing remote sensing imagery data that is commonly used today, although ground-based and aircraft platforms are also used. The unique characteristics of the satellite make it particularly useful for remote sensing of land surfaces. In this study, high-resolution Land Surface Temperature (LST) data for Sweden were derived from the MODIS Terra satellite (MOD11A2, Collection 6.1). The dataset provides 1 km resolution, 8-day composite LST. Daytime LST data were collected over five 8-day periods each year from 26 June to 5 August, covering the years 2015–2022. This period is chosen because it is the hottest period in the summer season for most regions in Sweden, according to SMHI [85], it is a favourable period for collecting LST data with minimal cloud coverage and extensive surface data coverage. The time series data with average LST temperature was used in this study. The data obtained on LST were pre-processed using QGIS and Python programming. Preprocessing, like data engineering, classification, and raster calculations, was done to obtain the final LST map.

Population and building data

Statistical data for population and the number and age of residential and single-family houses (SFH) in each of the 290 municipalities were collected from Statistics Sweden (SCB) database [19]. According to the population data of 2022 from SCB [19], Sweden has a population of about 10 million, out of which 20 % are over 65 years. This group of elderly people are considered a vulnerable group to SUHI and heat-related risks [82]. The building stock data, including the year of construction and the number of residential buildings taken from [19] is shown in the Table 2. There are 4.8 million residential dwellings, out of which 2.1 million are SFH, including one or two dwellings. About 80 % of the SFH stock (i.e. 1.58 million SFH houses) was built before 1980, which makes this sector responsible for a high portion of energy consumption and greenhouse gas emissions [19]. Building typologies and information on common SFH were extracted from the TABULA database [86]; U-values for the walls, roof, windows, doors, and floors were among the data acquired on building energy performance that led to the identification of five different typologies for SHF. The shape files for the building's footprint distribution across Sweden, and population distribution by localities of Sweden are obtained from the OpenStreetMap (OSM) database [87].

Assessing and mapping risk components

Assessing and mapping of SUHI Intensity (hazard)

Mapping SUHI intensity involves several steps to understand the intensity and spatial distribution of elevated temperatures in urban areas. Initially, LST imagery was collected and pre-processed to ensure consistency and compatibility. The pre-processing of data includes georeferencing, reprojection, clipping to the Swedish area, and defining no data values of LST imagery to be masked and excluded from calculations. Then, deriving LST values in degrees Celsius by applying a correction (scaling) factor and converting from Kelvin as given by Eq. (1) [88].

$$\mathrm{LST}(^{\circ}\mathrm{C}) = \mathrm{LST}_{\mathrm{MODIS}}(^{\circ}\mathrm{K}) \times \alpha - 273.15 \quad (1)$$

where α is the correction (scaling) factor, $\alpha = 0.02$. This correction factor is needed to account for anomalies in data due to technological problems and cloud contamination [88].

The next step is to obtain the map of LST for urban and rural areas. For that, land use and land cover imagery data (CORIN) from the Copernicus database are used, in which rural and urban classes are extracted. Hence, the intersection is applied between the LST map and the obtained urban and rural shapefiles to get LST maps for urban and rural. Urban pixels were defined using the city boundary polygon, while rural pixels were identified as non-urban areas within a 5-kilometre buffer surrounding the city. The final step is extracting the LST map for rural and urban areas for the 290 municipalities to get accurate SUHI values. For each municipality, the mean value of LST for rural areas is evaluated. Finally, SUHI intensity is calculated for each grid cell of the urban area by substituting the mean LST of rural areas from the Urban LST for each municipality, as illustrated in Eq. 2 [79].

$$SUHI_{Municipality}(^{\circ}\mathrm{C}) = LST_{Urban}(^{\circ}\mathrm{C}) - LST_{Mean\_Rural}(^{\circ}\mathrm{C}) \text{ for } 290 \text{ municipalities} \quad (2)$$

Finally, all the resulting 290 SUHI maps are merged to obtain the SUHI for the whole territory of Sweden.

Assessing and mapping exposure

Separate maps for building footprint distribution and population distribution by localities across Sweden were created using QGIS. The shape files for building footprint distribution across Sweden were obtained from Open OpenStreetMap (OSM) database [87], and population distribution by localities of Sweden is obtained from the SCB database

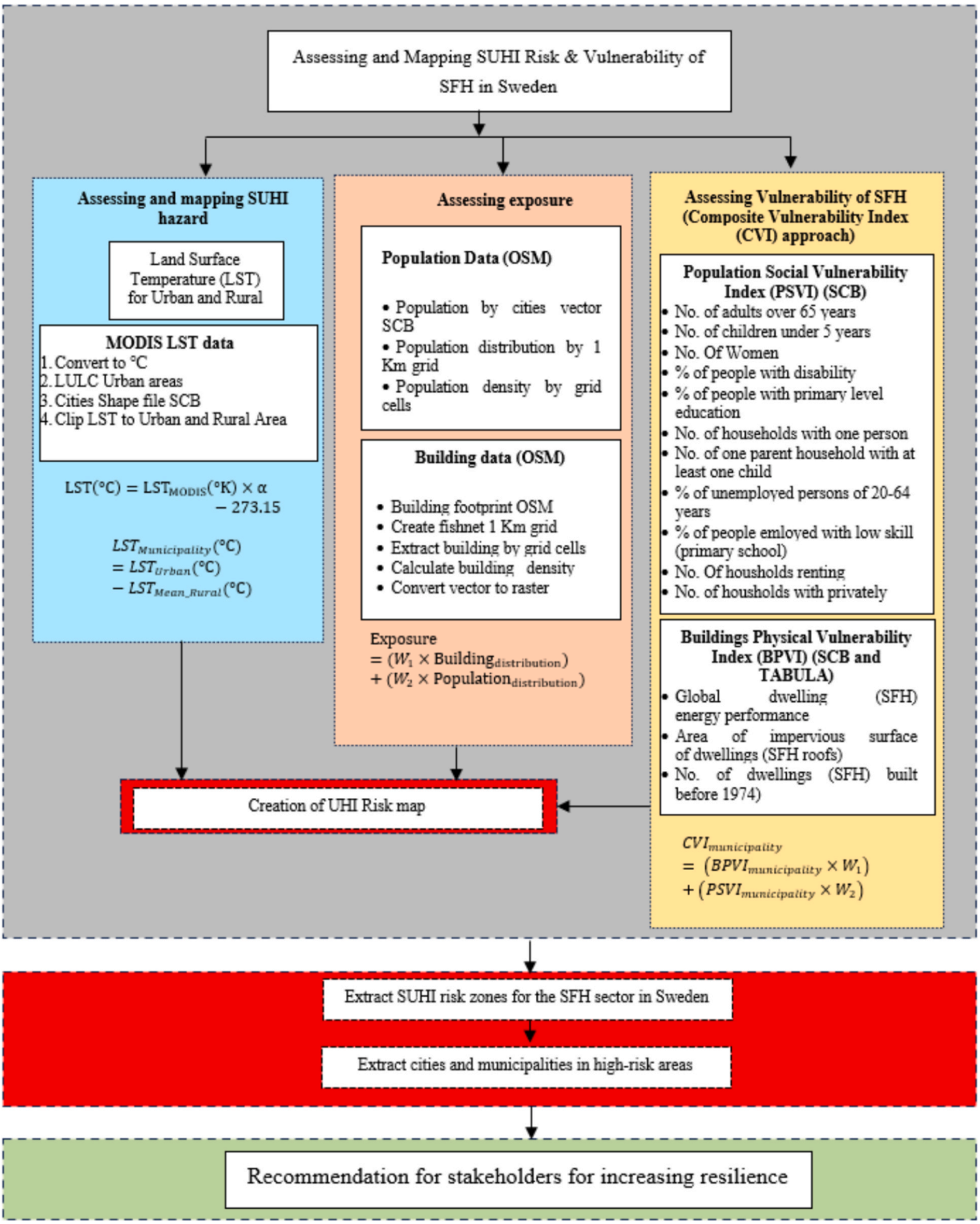


Fig. 2. Framework for assessing and mapping UHI risk in the SFH sector (developed by authors and adapted from the risk frameworks from IPCC AR5 [82,83]).

[19]. The exposure map was created by weighted summing of the two maps as shown in Eq. (3). Only buildings and population maps were used to measure exposure because they are the study's target elements.

$$\text{Exposure} = (W_1 \times \text{Building}_{\text{distribution}}) + (W_2 \times \text{Population}_{\text{distribution}}) \quad (3)$$

Assessing and mapping vulnerability

Following the risk assessment framework in IPCC's AR5 [82], a Composite Vulnerability Index (CVI) was developed and evaluated for 2,017 cities across the 290 municipalities of Sweden. The CVI is assessed by combining two components: the Population Social Vulnerability Index (PSVI) and the Building Physical Vulnerability Index (BPVI), both

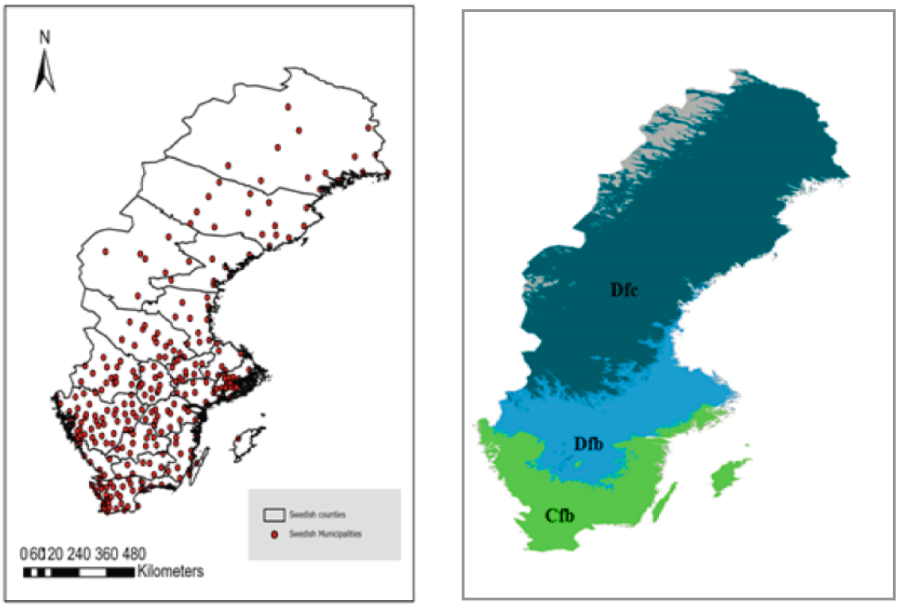


Fig. 3. The map of Sweden includes the boundaries of (a) 21 counties and 290 municipalities, and (b) Köppen climate zones [84].

Table 2
Proportion of the building stock in Sweden.

Year	Residential		Non-Residential
	SFH	Multi-dwelling buildings	Other buildings
−1930	417,909	214,082	16,831
1931–1940	140,763	158,105	5332
1941–1950	137,673	245,918	4607
1951–1960	164,890	399,711	8627
1961–1970	290,434	583,569	11,014
1971–1980	427,257	299,618	6942
1981–1990	216,088	196,463	6299
1991–2000	99,596	127,645	3788
2001–2010	115,262	114,150	4481
2011–2020	89,926	264,906	4936
2021–2022	16,238	65,893	373
data missing	9233	5209	6385
Total SFH	2,125,269	2,675,269	79,615
Before 1980 s	1,578,926	1,901,003	53,353

of which are calculated using a set of sensitivity and adaptive capacity indicators. The PSVI was calculated using 13 indicators, while the BPVI was based on 3 indicators, making a total of 16 indicators. These indicators are categorised by domain and dimension as detailed in the Table 3.

Data for most of these indicators are obtained from SCB statistics, except global dwelling energy performance is evaluated using the number of buildings and their global U-value as given in Eq. (4). The number of SFH collected from SCB is categorised into five classes according to the buildings' typologies in the TABULA database [86] as shown in the Table 3. For each category, the building's U-value and area are defined for the building envelope, including roof, walls and windows. The building's U value of each class was evaluated by the area-weighted average of each building envelope component's U value as. Although the SUHI effect on the energy performance of residential buildings is demonstrated in some studies, like [89], the incorporation of this indicator in evaluating community vulnerability to heat risks is rarely discussed (Table 4).

$$U_{building} = \frac{(U_{wall} \times A_{wall}) + (U_{roof} \times A_{roof}) + (U_{window} \times A_{window})}{A_{wall} + A_{roof} + A_{window}} \quad (4)$$

It is accepted that the higher the overall U value for the building, the more it is vulnerable to SUHI intensity. Therefore, according to the calculated U values, the buildings constructed before the 1960s are to be more vulnerable to SUHI intensity than those built between 1960 and 1975 and so on. The SFH global energy performance for each municipality is calculated based on Eq. (5).

$$SFH_{Globalenergyperformance} = \sum_{i=1}^{5} \left(U_{b,i} \times b_{municipality}\right) \quad (5)$$

where, $b_{municipality}$ is the number of buildings in each building class, $U_{b,i}$ is the U value of each building class.

The BPVI at each municipality is calculated using Eq. 6.

$$BPVI_{municipality} = \sum_{i=1}^{3} (BPV_i \times W_i) \, for\, each\, municipality \quad (6)$$

where i is the number of building physical vulnerability indicators, BPV is the Building Physical Vulnerability, and W is the allocated weight for each indicator.

Similarly, the PSVI at each municipality is calculated using Eq. 7.

$$PSVI_{municipality} = \sum_{j=1}^{13} \left(PSV_j \times W_j\right) \quad for\, each\, municipality \quad (7)$$

where j is the number of population social vulnerability indicators, PSV is the Population Social Vulnerability, and W is the allocated weight for each indicator.

Thus, the CVI at each municipality is calculated using Eq. (8).

$$CVI_{municipality} = \left(BPVI_{municipality} \times W_1\right) + \left(PSVI_{municipality} \times W_2\right) \quad (8)$$

Assessing the weights of indicators

In the literature, the equal weighing method, entropy method, Principal Component Analysis (PCA) method, analytical hierarchical process, expert weighing methods, slope-weighted method, and factor weighing method are different weighing methods used to allocate

Table 3
Vulnerability Indicators.

Indicator code	Indicator	Domain	Dimension	Rationale	Index	Effect on Vulnerability
Population Social Vulnerability (PSV)						
PSV_1	No. of adults over 65 years of age	Age	Sensitivity- Dwellers	Older adults are more vulnerable to the effects of urban heat	PSVI	+
PSV_2	Number of Children under 5 years of age	Age		Physiologically, the young have a greater susceptibility to the effects of UHI.	PSVI	+
PSV_3	Number of Women	Gender		Physiologically, women have a greater susceptibility to the effects of extreme heat.	PSVI	+
PSV_4	Percentage of People with a disability	Health		Physiologically, those with a disability have a greater susceptibility to the effects of extreme heat.	PSVI	+
PSV_5	Percentage of People with a primary school level	Education/ Information Access/ Use	Adaptive Capacity – Ability to Prepare/ Respond	People with no formal education may find it difficult to interpret and/or act on information received	PSVI	+
PSV_6	Number of Households with one person	Social Network		Those living alone likely lack a support network that can assist them during a heatwave event	PSVI	+
PSV_7	Number of one-parent households with at least one child	Income		One-parent households are more likely to have less disposable income compared to other households	PSVI	+
PSV_8	Percentage of Unemployed persons of 20–64 years			Unemployed persons are more likely to have lower incomes, and have limited ability to make physical adjustments to their property to adapt to extreme heat	PSVI	+
PSV_9	Percentage of low-skilled (primary school) employed persons			People in low-skilled employment are likely to have less income, reducing their ability to adapt before, during, or after an event.	PSVI	+
PSV_10	Number of Households renting	Tenure		Renters are more likely to have lower incomes, plus have limited ability to make physical adjustments to their property to adapt to UHI.	PSVI	+
PSV_11	Number of Households with Private Ownership	Ownership		Privately owned householders are more likely to have larger incomes plus have a strong ability to make physical adjustments to their property to adapt to UHI.	PSVI	–
PSV_12	Number of persons with privately owned cars (per 1000 inhabitants)	Mobility		No personal access to a vehicle may increase exposure to the UHI event	PSVI	–
PSV_13	Number of foreign citizens	Local knowledge		Foreign nationals are likely to have less local knowledge and be less aware of hazards	PSVI	+
Building Physical Vulnerability (BPV)						
BPV_1	Global dwelling (SFH) energy performance (walls, roofs and windows)	Housing Characteristics/ Performance	Sensitivity- Dwellings	Low-performance buildings increase the cost of response to extreme heat events	BPVI	+
BPV_2	Area of Impervious surface of dwellings (SFH roofs)	Housing Characteristics/ reflectance		Increased areas of impervious surface and non-vegetated areas enhance the impacts of UHI	BPVI	+
BPV_3	Number of dwelling (SFH) built before 1975)	Housing Characteristics/Age		Households built prior to 1975 or 1945 may be of poor quality and may not offer as much protection to residents when compared to modern housing	BPVI	+

Table 4
Characteristics of building typologies [86].

Parameter	U-Value (W/m^2. °C) building class					Area (m^2)
	Class1 (1920–1960)	Class2 (1961–1975)	Class3 (1976–1985)	Class4 (1986–1995)	Class5 (1996–2005)	
Roof	0.29	0.21	0.15	0.12	0.12	125
External wall	0.6	0.31	0.21	0.17	0.2	100
Window	2.34	2.3	2.01	2.0	1.87	22

weight for indicators. The contrasting findings regarding the effectiveness of weighing methods illustrate the importance of the context-specific approach [90]. In this work, two data-driven methods (PCA and entropy weighting methods) were investigated for calculating the weights of indicators. But after comparison, only one of them is selected for developing the maps of risk components.

It is noted that all indicators were normalised using Min-Max and Z-score normalisation methods, as shown in Eq. (9) and Eq. (10) respectively. Min-Max normalisation was applied before the entropy weighting method, while Z-score normalisation was used before applying the PCA weighting method.

$$X = \frac{x - x_{min}}{x_{max} - x_{min}} \tag{9}$$

$$X = \frac{x - \mu}{SD} \tag{10}$$

where X is the normalised value for the given feature, x is the original value of the feature, x_{min} and x_{max} are the maximum and minimum values of the dataset. SD is the standard deviation, and μ is the mean of the given dataset.

Assessing and mapping SUHI risk

To identify areas where the SFH sector is at high or medium risk from SUHI effects, the resulting maps of SUHI intensity (hazard), exposure, and vulnerability were combined using various weighting methods. This process was carried out using Python and QGIS, based on Eq. (11).

$$SUHI_{risk} = (\text{SUHI intensity} \times W_1) + (\text{Exposure} \times W_2) + (\text{Vulnerability} \times W_3) \quad (11)$$

where W_1, W_2 and W_3 are the weights assigned to risk components. It is noted that all three components of risk are normalised through minmax normalisation before performing raster calculation to get the final risk map.

Assessing the weights of risk components and sensitivity analysis

In this study, a comparative analysis was conducted to assess the influence of different weighting methods on the final SUHI risk assessment. Five approaches were tested, including entropy-based data-driven weighting, equal weighting, and three methods that prioritised hazard, exposure, and vulnerability components individually. PCA-based weighting was excluded from the final comparison due to abnormal Z-score distributions in the hazard maps, which led to inconsistent or non-interpretable results. Each method produced a distinct risk map, and their performance was evaluated using heat-related mortality data as a proxy for validation. The most suitable weighting method was selected based on its ability to accurately identify a greater number of counties with recorded deaths within high-risk zones, while also correctly classifying counties without recorded deaths as low-risk areas. Fig. 4 illustrates the validation process used to select the most appropriate weighting method for SUHI risk mapping.

Identification of municipalities and cities at risk to SUHI

The primary goal of most climate risk assessment and mapping studies is to identify elements at risk, assess potential impacts or losses, support the development of adaptation and mitigation strategies and provide actionable information to stakeholders. In this study, the aim is to offer useful insights to stakeholders, mainly municipal policy makers, to support planning efforts that enhance the resilience of Sweden's building sector and vulnerable population to heat-related stress, with a focus on the SUHI effect. After selecting the most appropriate weighting method for combining risk components and identifying high-risk areas, the study proceeds to identify and analyse the municipalities and cities located within these zones. This step is essential for informing decision makers about the areas mostly at risk. It also provides a foundation for recommending targeted strategies to improve the resilience of the single-family housing (SFH) sector and reduce SUHI intensity, contributing to both environmental and socio-economic benefits. Municipalities where SFHs are at high risk from SUHI were identified using the "Select by Location" tool in QGIS, by intersecting the high-risk zone vector map with the cities vector map. The resulting list of municipalities was then exported as a CSV file for further analysis in Excel.

Results and discussions

After compiling all necessary datasets and conducting data analysis and spatial computation, the maps for indicators are developed. In addition, the weights for indicators and risk components are also evaluated and used for developing maps for risk components and the final SUHI risk map.

Resulting weights for indicators and risk components

Weights for PSVI and BPVI related indicators

The obtained weights for PSVI and BPVI related indicators through PCA and entropy methods are given in the Table 5.

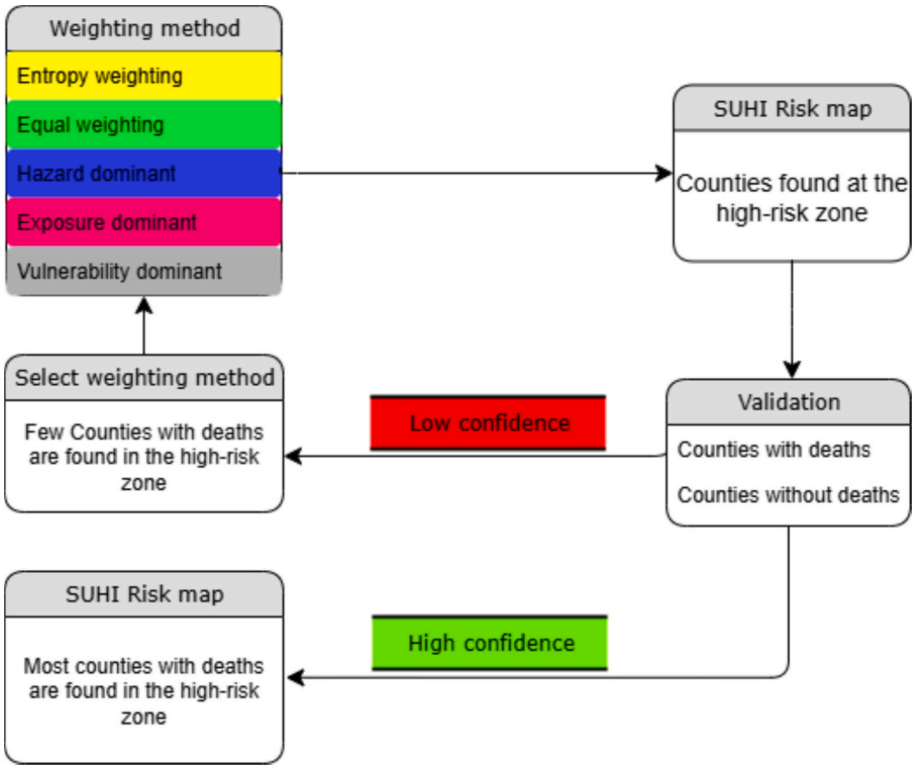


Fig. 4. Validation process for selecting the appropriate weighting method.

Table 5
Weights for PSVI and BPVI related indicators.

Indicator code	PSV-related indicator	PCA Weights	Entropy Weights
Weights for PSVI-related indicators			
PSV_1	number of adults over 65 years of age	56.98	10.03
PSV_2	Number of Children under 5 years of age	16.16	13.43
PSV_3	Number of Women	8.93	12.97
PSV_4	Percentage of People with a disability	6.09	5.17
PSV_5	Percentage of People with a primary school level	5.58	0.99
PSV_6	Number of Households with one person	3.42	14.22
PSV_7	Number of one-parent households with at least one child	1.36	13.92
PSV_8	Percentage of Unemployed persons of 20–64 years	1.22	1.86
PSV_9	Percentage of low-skilled (primary school) employed persons	0.18	1.36
PSV_10	Number of Households renting	0.05	6.66
PSV_11	Number of Households with Private Ownership	0.01	0.19
PSV_12	Number of persons with privately owned cars (per 1000 inhabitants)	0	1.38
PSV_13	number of foreign citizens	0.02	17.8
Weights for BPVI-related indicators			
BPV_1	Global dwelling (SFH) energy performance	97.62	29.37
BPV_2	Area of Impervious surface of dwellings (SFH roofs)	2.3	41.44
BPV_3	Number of dwellings (SFH) built before 1975)	0.08	29.2

Weights for composed vulnerability index indicators

As discussed in Section 3, the weights for the exposure indicators were calculated using both PCA and the entropy weighting method. These weights were used to generate the exposure map, as shown in the Table 6. Similarly, the Composite Vulnerability Index (CVI) was developed by combining the Building Physical Vulnerability Index (BPVI) and the Population Social Vulnerability Index (PSVI) using a weighted sum approach. The weights for BPVI and PSVI were also derived using PCA and entropy methods to ensure a data-driven and systematic assessment of vulnerability. The complete set of weights used for both exposure and vulnerability components is presented in the Table 6.

The exposure and vulnerability maps were created using entropy-based weights, as this method offers a more balanced way of assigning importance to indicators compared to PCA. We chose entropy weighting because our dataset included indicators with skewed distributions and outliers. For example, some Z-scores ranged from −2 to 30, and population data had extreme values for large cities like Stockholm. PCA is sensitive to such outliers and assumes normal data distribution, which can lead to unreliable results. In contrast, the entropy method does not require normality and works well with skewed or bounded data [91].

Weights for risk components

After getting the weights of all indicators using both PCA and entropy methods, the maps for the three components of risk (hazard, exposure and vulnerability) were developed. In this study, the maps of risk components were created using the resulting weights from the entropy weighting method, as they provided a more balanced and contextually appropriate representation. The final SUHI risk map was then generated by applying a weighted sum of the three component maps.

To evaluate the influence of different weighting schemes, a sensitivity analysis was conducted using several alternative methods. The resulting weights for hazard, exposure, and vulnerability from each method are summarised in the Table 7. Based on these methods, five distinct SUHI risk maps were produced and are presented in the following sections.

Table 6
Weights for BPVI-related indicators.

CVI-related indicators	PCA weights	Entropy weights
For Exposure Indicators		
Building density distribution	78 %	44 %
Population density distribution	22 %	56 %
For Vulnerability Indicators		
BPVI	50 %	47 %
PSVI	50 %	53 %

Mapping hazard

In this study, SUHI intensity is used to represent the hazard component. The final SUHI intensity map was developed primarily using pre-processed Land Surface Temperature (LST) satellite imagery, complemented by Land Use and Land Cover (LULC) data for Sweden.

Mapping Land Surface Temperature (LST)

LST satellite imagery maps for the years 2015–2022 for Sweden are shown in Fig. 5 (a) to (h), along with the resulting average LST map (average of the years 2015 to 2022), presented in Fig. 5 (i). These maps visualise surface temperature distributions across the country, with warmer areas shown in darker orange/red and cooler areas in yellow. The data reveal consistent spatial patterns, where the southern and central parts of Sweden experience higher surface temperatures, likely due to urbanisation and land use intensity (especially the bigger cities like Göteborg and Stockholm), while northern regions remain cooler. Annual variations are noticeable, reflecting inter-annual climate fluctuations. The average LST map (Fig. 5 (i)) smooths out short-term variability, offering a clearer view of persistent surface temperature patterns over the years. The LST spans from approximately 0 °C (yellow), corresponding to high-latitude plateaus and mountainous terrain in northern and central Sweden, to 30 °C (deep orange/red) in the warmest lowland and coastal zones. A pronounced north–south gradient is evident: southern and coastal municipalities, particularly around major urban agglomerations, exhibit the highest LST, whereas the sparsely settled boreal interior and mountain range remain substantially cooler.

The above resulting LST maps include all LULC classes, but only urban areas should be included in the assessment and analysis of SUHI intensity and risk. Thus, the filtered average LST map for urban areas (excluding some land use classes such as water bodies) is generated as presented in Fig. 6 (a). It presents the average LST for urban areas across Sweden, highlighting regional variations in LST. The two zoomed-in sections highlight the contrast between the northern and southern regions of Sweden. The upper inset shows the northern region, where sparse urban areas correspond to moderate surface temperatures and limited urban heat buildup. In contrast, the lower inset shows the southern region, where denser urban development and impervious surfaces may have resulted in significantly higher surface temperatures. The observed variations in LST across Sweden are influenced by several factors: differences in the extent of built-up areas, land use and land cover types (including soil characteristics), latitudinal range (as each climate zone spans varying distances from north to south), and elevation (with higher mountainous terrain in the northwest). Additionally, variations in solar radiation, both in duration and intensity, among the three climate zones contribute to the spatial differences in LST. Fig. 6 (b) illustrates the relationship between 1 km grid building density and mean land surface temperature (LST). The upward-sloping regression line (with 95 % confidence band) demonstrates that denser built-up areas tend to register higher surface temperatures. The widespread occurrence of individual points around the trend also highlights the influence of additional factors on LST variability.

Table 7
Weights of risk components by the weighting method.

Risk component /Weighting method	Entropy weights	Equal weights	Hazard dominant	Exposure dominant	Vulnerability dominant
SUHI Intensity (Hazard)	5 %	33 %	50 %	25 %	25 %
Exposure	26 %	33 %	25 %	50 %	25 %
Vulnerability	69 %	33 %	25 %	25 %	25 %

Mapping SUHI intensity

The filtered map of average land surface temperature (LST) for urban areas in Sweden served as the basis for generating SUHI intensity maps for all 290 municipalities, resulting in a total of 290 individual SUHI intensity maps. These were then merged to produce a comprehensive SUHI intensity map for the entire country. Additionally, SUHI intensity maps were developed for each of Sweden's three climate zones to enable more detailed, region-specific analysis.

Fig. 7 presents the SUHI intensity map for Sweden, illustrating how urban areas experience elevated surface temperatures compared to their rural surroundings. The zoomed-in views emphasise regions where intense SUHI effects are observed, particularly due to concentrated urban infrastructure and limited vegetation.

To provide a clearer spatial understanding, Fig. 8 displays SUHI intensity maps disaggregated by Sweden's climatic zones. In climate zone 1 (northern region), SUHI intensity is generally low. This can be attributed to sparse urban development, abundant forest cover, and a cooler overall climate that limits heat accumulation. In climate zone 2 (central region), a moderate SUHI intensity is observed, reflecting a mix of ongoing urban expansion and partial vegetation loss, both contributing to a rise in surface temperatures. The southern region (climate zone 3) demonstrates the highest SUHI intensity, driven by high urban density, widespread impervious surfaces, and limited forest coverage. These zonal differences highlight the influence of land use, vegetation cover, and urbanisation patterns on SUHI intensity across Sweden's diverse climatic regions.

The spatial patterns of SUHI observed in these maps closely align with Sweden's land use/land cover (LULC) distribution. As shown in Fig. 9, areas characterised by dense forests and water bodies exhibit lower SUHI due to their natural cooling effects, whereas highly urbanised regions, especially in the south, display higher SUHI intensity due to the limited presence of cooling vegetation and water surfaces. The highest recorded SUHI intensity approached **6.9 °C**, depicted in dark red on the map, indicating urban areas that retain significant heat. In contrast, the lowest SUHI values, approaching −2.3 °C, are shown in yellow and represent natural or rural landscapes with minimal heat retention.

These findings demonstrate substantial spatial variation in SUHI intensity between Sweden's southern and northern regions. The southern coastal areas consistently exhibit higher SUHI intensity, a phenomenon likely due to warmer temperatures and stronger solar radiation in the south compared to the north. Notably, variations are also observed between eastern and western regions, even within the same climate zone or latitude. This can be explained by differences in physical geography, such as the eastern coastline, the Scandinavian Mountain range in the west, and variability in infrastructure density, particularly around major cities.

To assess the accuracy of the calculated SUHI values, each municipality's SUHI was compared with theoretical values derived from studies conducted in other cities within the same climatic zone [80,92,93,94]. Fig. 10 presents a comparative analysis of calculated SUHI intensities across Swedish municipalities, stratified by Köppen–Geiger climate zone, with reference values from the literature overlaid for validation [92,93,94]. In the Cfb zone (temperate oceanic), calculated SUHI intensities are generally centred around the reference value of ~2.5 °C yet exhibit significant dispersion. High outliers, including Malmö, Lund, Burlöv, and Sundbyberg, exceed 5 °C. These municipalities are characterised by compact urban form, high building density, extensive impervious surface cover, and sparse vegetation, all of which contribute to increased surface heat retention. Malmö and Lund, for instance, have undergone rapid densification and vertical development, while Sundbyberg is among Sweden's most densely built municipalities. These morphological attributes may be insufficiently represented in the literature benchmarks, which tend to be based on average urban forms rather than extreme cases. Furthermore, temporal inconsistencies in the underlying satellite-derived LST datasets and possible differences in acquisition times (e.g., diurnal vs nocturnal SUHI) may also contribute to the observed deviations.

The Dfb zone (humid continental), which encompasses much of central Sweden, exhibits a narrower interquartile range, with SUHI values more symmetrically distributed around the literature reference of 3 °C. This suggests a more uniform urban structure and vegetation characteristics across municipalities in this zone. The slightly higher RMSE (1.58 °C) and CVRMSE (0.91) likely reflect moderate variations in urban expansion patterns rather than significant morphological discrepancies. Nevertheless, localised land cover heterogeneity, including mixed-use development and forest adjacency, may still modulate surface thermal profiles in certain municipalities.

In contrast, the Dfc zone (subarctic) demonstrates the widest spread in calculated SUHI values relative to its literature benchmark (~2.0 °C). Several municipalities fall well outside the expected range, with Borlänge identified as a notable high outlier. This variation may stem from a combination of factors: (i) lower baseline urbanisation levels leading to less thermal buffering, (ii) increased influence of surrounding forest and water bodies, (iii) persistent snow cover and high albedo surfaces affecting surface emissivity, and (iv) classification errors due to the lower thermal contrast between built-up and vegetated areas in cold climates. The high CVRMSE of 3.03 in this zone indicates that traditional models struggle to capture SUHI dynamics in sparsely urbanised, climatically extreme regions, suggesting the need for zone-specific model calibration incorporating snow-melt dynamics, seasonal vegetation indices, and industrial land use.

These discrepancies reflect the distinct morphological and land cover characteristics of outlier municipalities. Malmö, Sundbyberg, and Borlänge, all high-density urban centres with a high proportion of built-up area relative to vegetative cover, consistently show calculated SUHI values that exceed literature benchmarks. This may be partially attributed to the urban surface configuration, where extensive imperviousness and minimal vegetation increase surface heat storage and reduce nocturnal cooling. However, it also points to potential methodological inflation of SUHI estimates in highly urbanised environments. Specifically, the use of satellite-derived LST products, which capture radiometric rather than ambient air temperatures, can disproportionately register elevated surface temperatures in compact urban grids during clear-sky conditions. This highlights the need for caution when interpreting SUHI magnitudes in densely built municipalities, where exaggerated thermal contrasts with surrounding rural baselines may overstate the urban thermal burden. These findings underscore the value of integrating fine-scale urban land cover data such as vegetation fraction, building height, and surface albedo into SUHI modelling, particularly for spatially heterogeneous urban regions. Tailoring model inputs to account for urban form and surface material properties is essential for improving SUHI estimation accuracy and for guiding spatially targeted climate adaptation strategies.

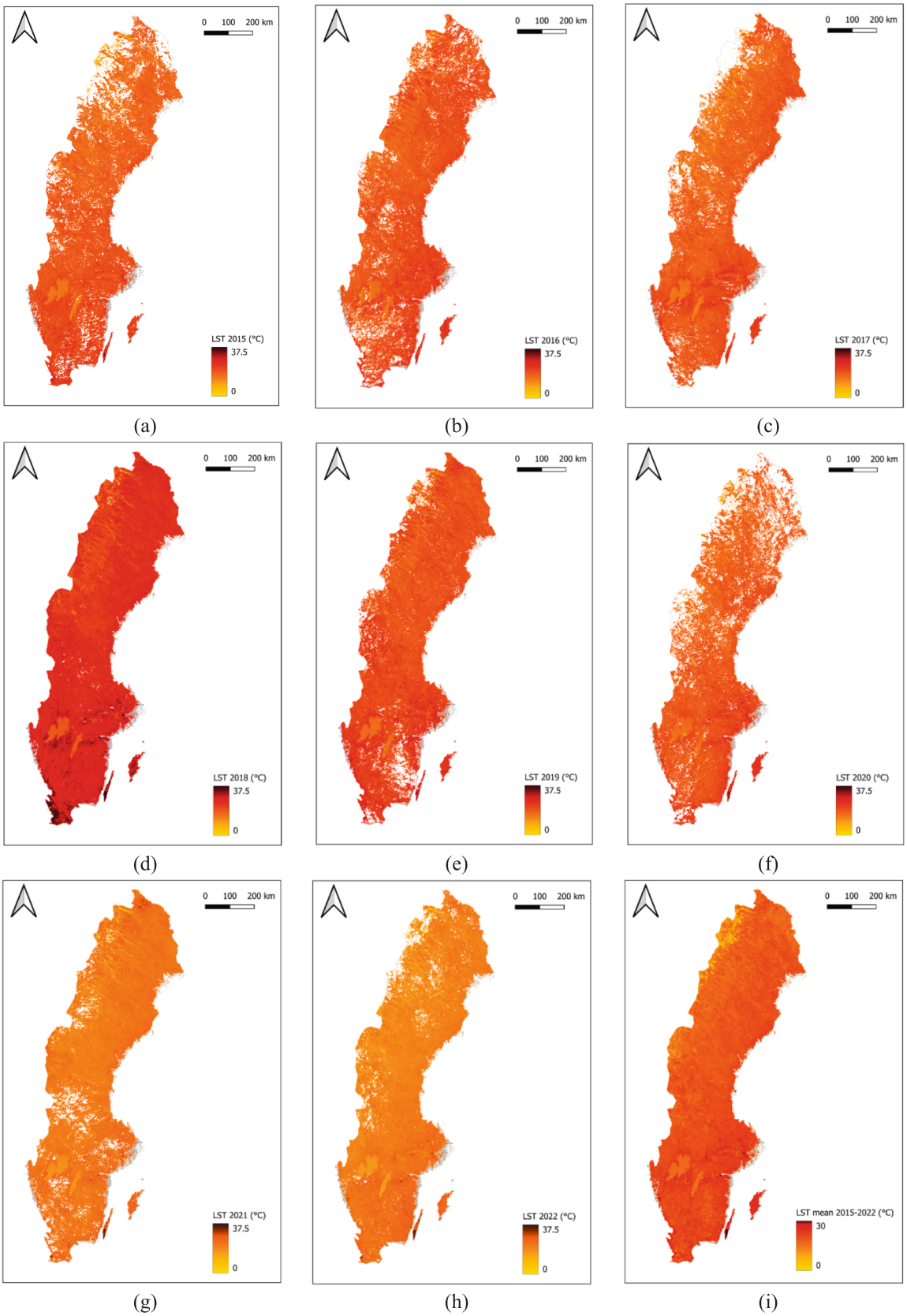
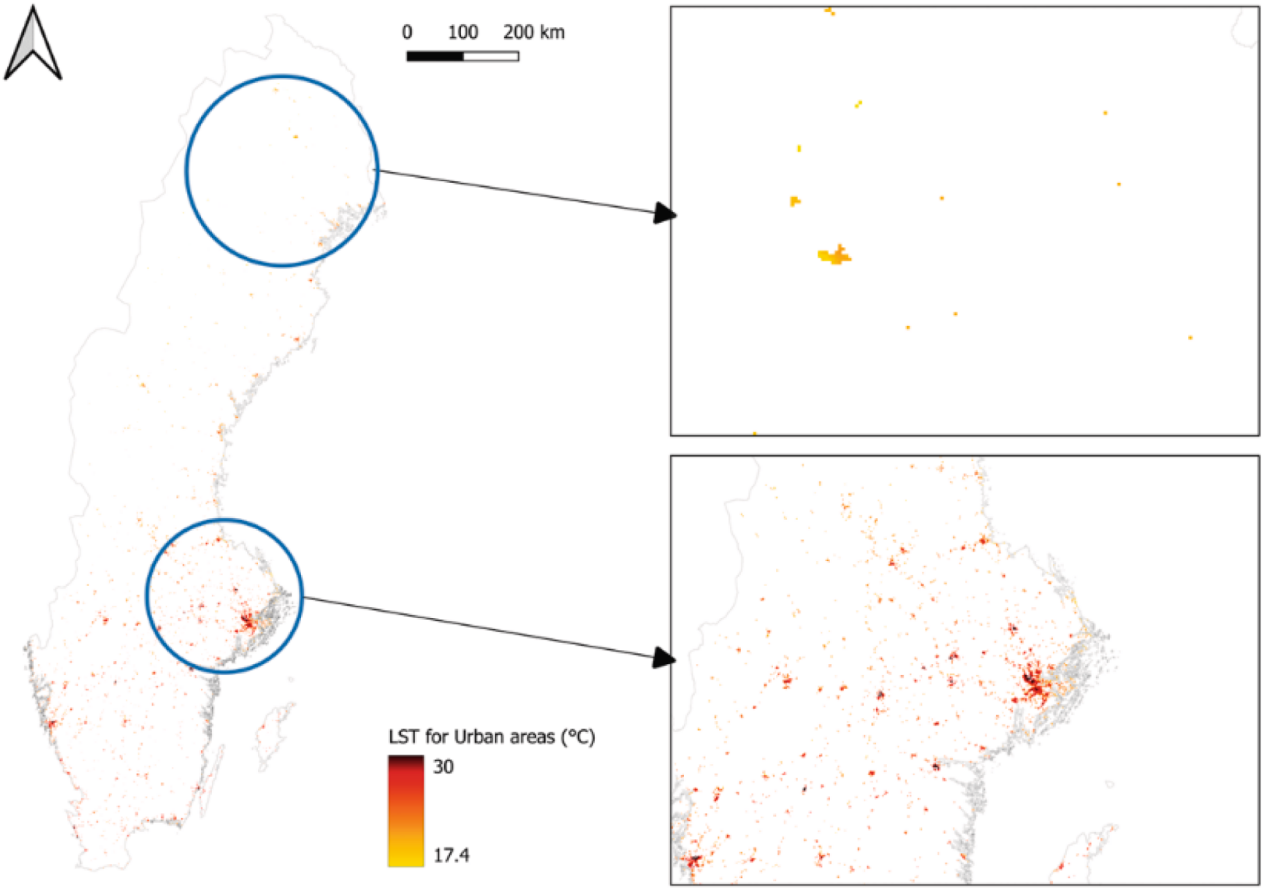
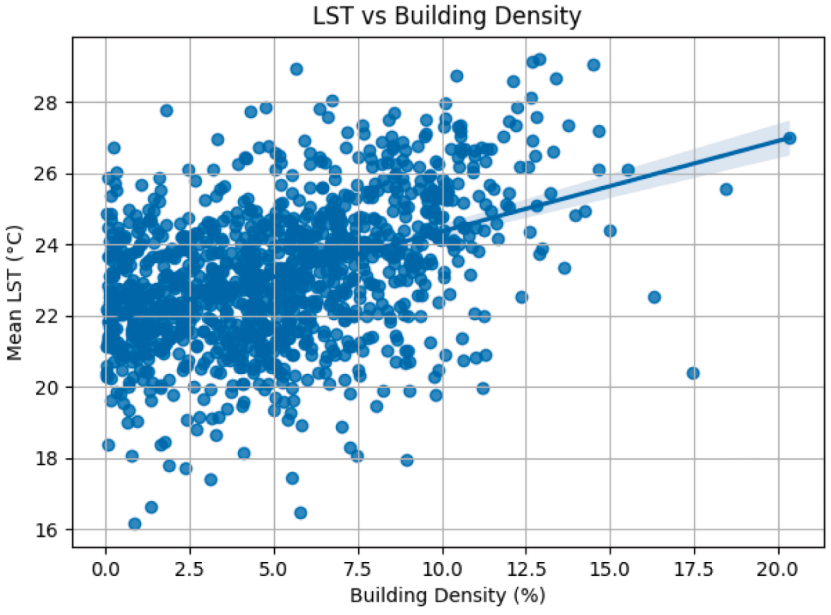


Fig. 5. LST satellite imagery maps for Sweden generated for each year from 2015 to 2022, labelled as (a) to (h), along with an additional map (i) showing the average LST over the entire 2015–2022 period.



(a)



(b)

Fig. 6. (a) The average LST for urban areas of Sweden and (b) Mean LST vs building density in percentage.

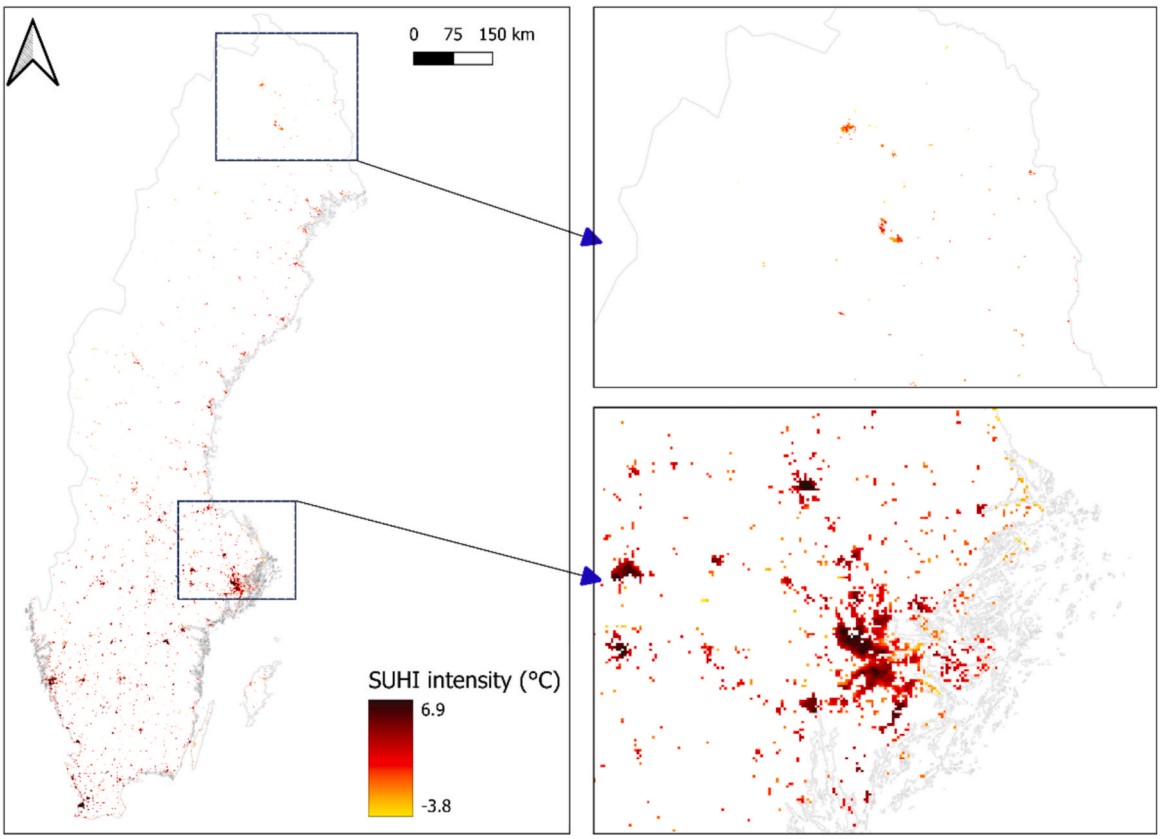


Fig. 7. SUHI intensity for Sweden.

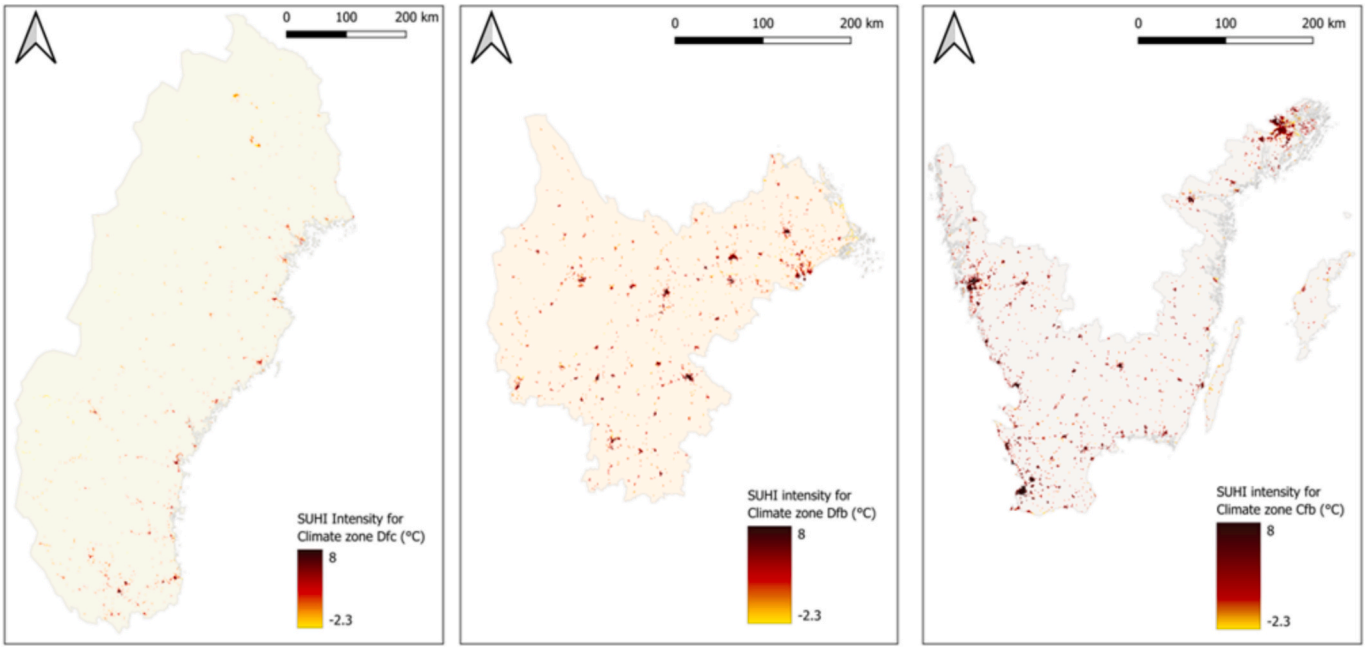


Fig. 8. SUHI intensity for each climate zone in Sweden.

Mapping exposure

Buildings and population distribution

The maps of 2D building footprints (based on OSM data) and Swedish population distribution (derived from SCB geodata for localities (2017 localities)) are combined for mapping exposure as shown in Fig. 11.

It shows that the southern part of Sweden is denser in buildings and population compared to the northern part, making it more exposed to climate risks. Within the southern part, the coastal regions, including major cities, are the most exposed. This increased exposure results from the urbanisation and extensive population migration to urban areas after

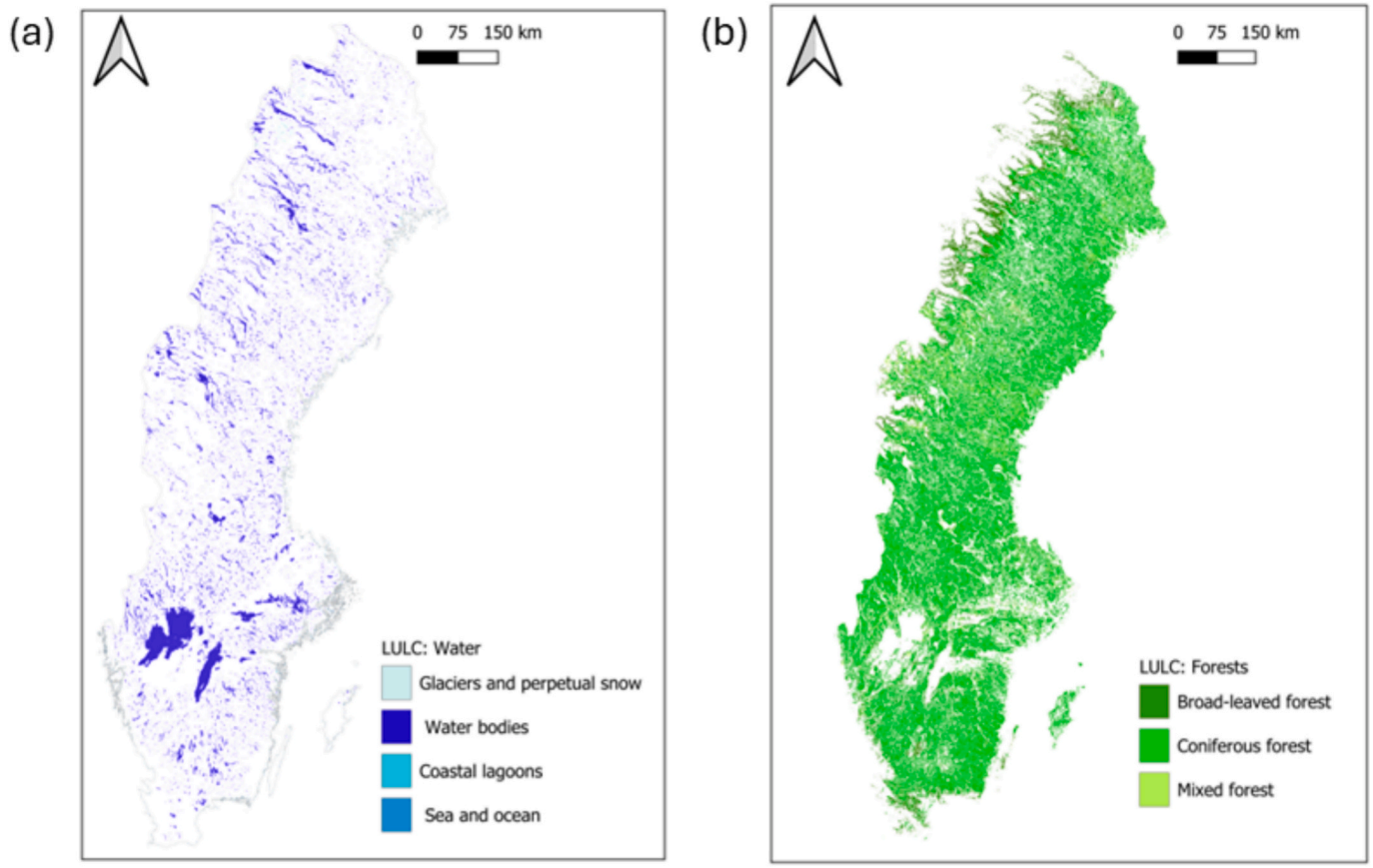


Fig. 9. LULC for Sweden: (a) water, (b) forests.

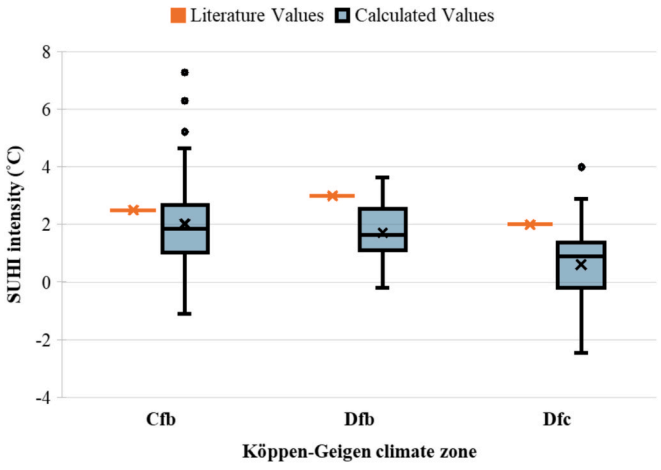


Fig. 10. Box plot comparing LST values obtained for all municipalities with literature values, with corresponding climate zones.

following the Million Hus program in Sweden, aided by the favourable climate in the southern location (which includes climate zones 1 and 2) for sustenance.

The population of Sweden is primarily concentrated in the central and southern regions, especially in coastal areas where most settlements are located. However, in the north, the northern regions have fewer settlements due to the extreme climate. However, certain areas in the north still have dense populations due to important activities such as mining and industries, as well as government financial support encouraging people to live there.

Buildings typically house the population, so their distribution mirrors that of the people. It should be highlighted that the area covered by the building is relatively large, which can be explained by the high ratio of living space per person. This is influenced by household preferences and lifestyle in Sweden, where large living areas are common for a few people. This factor can impact homeowners' ability to ensure adequate indoor thermal comfort, perform a deep renovation and maintain their large living homes regularly. Consequently, this increases their vulnerability to climate risks.

Mapping vulnerability

Mapping social and physical vulnerability indices

The maps for building physical vulnerability (based on BPVI) and population social vulnerability (based on PSVI) for the Swedish SFH sector by municipalities are presented in Fig. 12.

There is a similar trend in the locations of vulnerable populations and buildings, as older structures often house older individuals, reflecting historical settlement patterns. The Million Houses program from 1965 to 1974 facilitated migration from small towns and rural areas to major cities like Stockholm, Gothenburg, and Mälmö, which are situated in the southern coastal regions of Sweden. Therefore, these areas have a large stock of buildings built before 1975, now over 50 years old, with low thermal performance. This is the reason municipalities in these areas would be more susceptible to climate risks than those in other parts of Sweden. The large living areas of these buildings, combined with the high cost of renovation per m^2, and the lack of government financial support for renovation, prevent homeowners in these aged buildings from undertaking deep renovation.

By combining the PSV map and the BPV map, the map for SFH sector vulnerability by municipalities is created as shown in Fig. 13.

According to the generated vulnerability map, most municipalities,

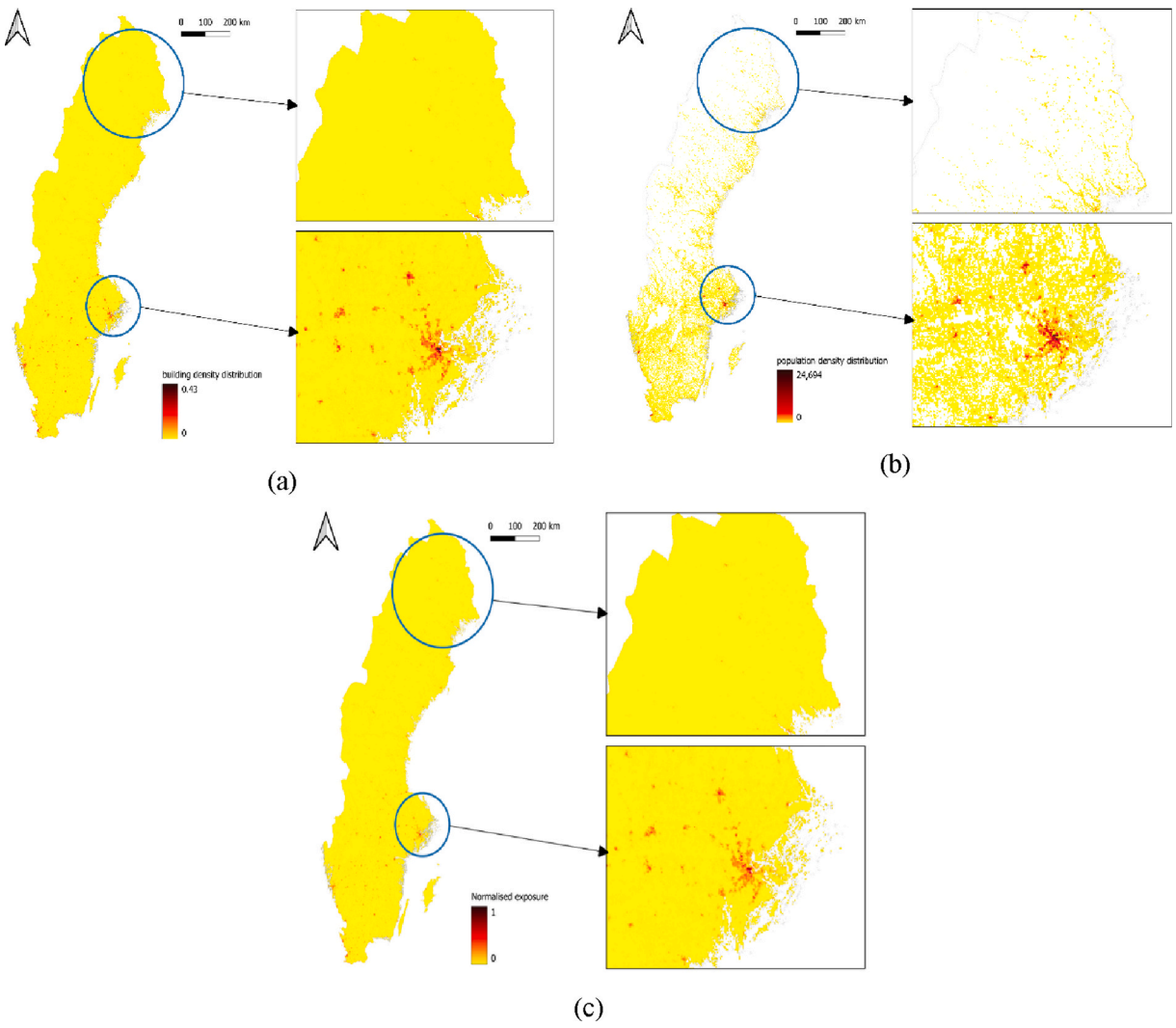


Fig. 11. (a) Buildings and (b) population density distribution, and (c) normalised exposure maps for Sweden.

particularly those in northern Sweden, are less vulnerable. However, certain municipalities on the southern coast, especially in the eastern parts, are significantly vulnerable, as they contain a large building stock built before 1975, and populated by elderly people. The factors contributing to this vulnerability include the comfortable environment, attractive nature, and extensive migration to these regions since the implementation of the Million House Program.

Mapping SUHI risk

Prior to identifying the specific cities and municipalities where the SFH sector faces elevated SUHI risk, we validated our weighting schemes against real-world health outcomes. Because mortality is widely regarded as the most critical indicator of heat-related health impacts [95], we obtained regional data on deaths attributable to extreme heat in Sweden from 1997 through 2023 [19]. We then compared the counties flagged as high-risk under each candidate weighting method with those that recorded heat-stress fatalities. The weighting approach, whose high-risk counties best matched the observed mortality patterns, was chosen to derive the final component weights for our SUHI risk index. Table 8. shows counties at risk by a weighting method for risk components and the number of deaths due to heat stress by county.

According to the obtained results, it can be concluded that the exposure dominant weighting method is the most appropriate weighting method for assigning the weights of SUHI risk components for Sweden. Because most counties located in high-risk are those who have deaths, and only two counties without any deaths are highlighted under risk (which means low failure). Thus, exposure exposure-dominant weighting method is applied to extract the cities and municipalities at high-risk to SUHI, to perform further data analysis and recommend strategies for enhancing the resilience of the SFH sector to SUHI.

Fig. 14 maps SUHI risk for Sweden's SFH sector by merging hazard intensity, housing exposure, and vulnerability under an exposure-dominant weighting scheme. It shows that the highest-risk zones are concentrated in the southern and coastal regions, particularly climate zones 2 and 3, where Sweden's largest cities and densest SFH clusters coincide with stronger SUHI effects. This southern concentration reflects both historical development (many SFHs there date from before 1975) and the population's preference for coastal living, which together drive high exposure and structural vulnerability. By contrast, western and northern areas (climate zone 1) remain sparsely populated despite targeted incentives for settlement, resulting in lower SUHI risk for their SFH sectors. A study in Italy [96] similarly highlights that the residents of coastal plain cities, with their mild climates and low daily temperature variations, are more vulnerable to sudden temperature shifts and extreme heat events. This is because such populations are less accustomed to high temperatures, making them less adaptable to sudden extremes. Moreover, a study by [97] in Italy noted that residents of coastal plain cities may be more susceptible to heat-related effects due to

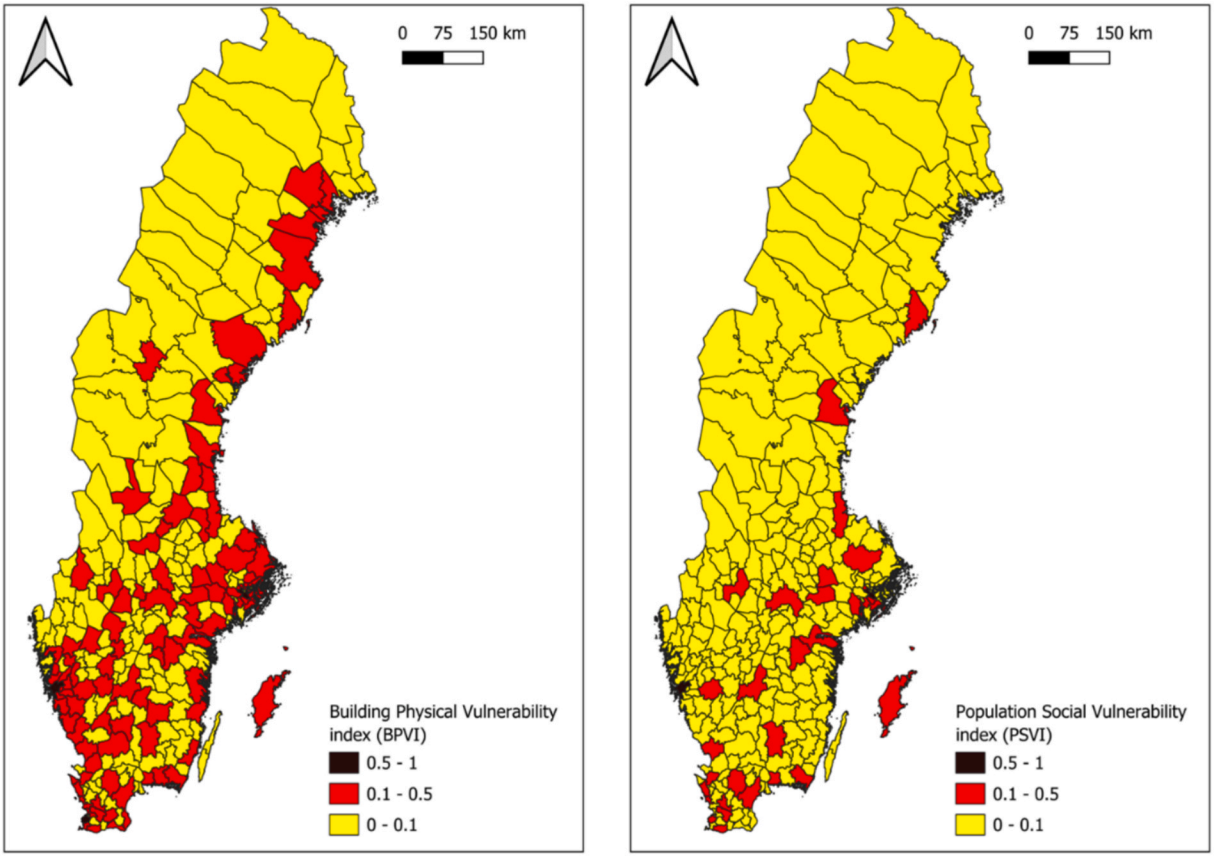


Fig. 12. Building Physical vulnerability and population social vulnerability for the Swedish SFH sector by municipalities.

the prevalence of extensive high-risk areas. Despite these parallels, a meaningful comparison with Italy must account for key contextual differences. Swedish coastal cities have cooler climates, modern urban planning, and strong institutional capacity focused on sea-level rise and rainfall management. In contrast, Italian coastal cities face hotter Mediterranean climates, historic urban forms with limited green space, and greater exposure to heatwaves and flooding, compounded by fragmented governance. Nonetheless, both Swedish and Italian coastal areas tend to be densely populated, since residents gravitate toward the coast, thereby increasing overall exposure to these climate risks despite their differing environmental and institutional settings.

These heightened risks have tangible implications: for example, insurance companies often limit or refuse coverage for homes in such high-risk areas. Given these challenges, it is crucial for the Swedish municipalities to prioritise targeted and immediate interventions to mitigate these risks. If a nationwide renovation initiative is undertaken, high-risk regions should be prioritised, with resources allocated strategically to maximise impact and resilience. Collaboration between municipalities, bankers, insurance and renovation companies will be essential to minimise the potential losses [98]. The cooperation modality for such efforts needs further exploration. Moreover, identifying municipalities at risk is a critical step in ensuring that resources and efforts are directed efficiently, as discussed in the following section.

Exploring cities and municipalities at risk to SUHI

Cities and municipalities in high risk of SUHI

Table 9 shows cities and municipalities where SFH is at high risk of SUHI in Sweden. Besides, Fig. 15 shows the geographical location of Swedish municipalities at high risk of SUHI. The figure illustrates that most municipalities where the SFH sector is at risk of SUHI are in the southern part of Sweden, with few municipalities on the western coast of the northern part. Overall, there are 12 municipalities in high-risk areas and 19 municipalities in medium-risk areas out of 290 municipalities in Sweden.

Based on the identified municipalities (12 of 290 municipalities) at high risk (see Fig. 15) and their associated population and SFH related statistics (see Table 10), as well as the assigned weights for each, it is concluded that the vulnerability indicators (mainly number of women, children under 5 years, and SFH characteristics mainly impervious surface area, age and energy performance), and exposure indicators (mainly total number of population that linked directly to the urban density) contribute significantly to high risk in these municipalities. It is also observed that more than 60 % of SFH in these 12 municipalities were built before 1975, which indicates that the age (and mostly are low energy performance houses, as the rate of renovation is very low in Sweden) makes these municipalities high-risk areas. These conclusions can also be supported by the fact that the urban dense municipalities in Sweden (including Stockholm, Göteborg, Malmö) are in the identified high-risk zone.

Fig. 16 reports, for each high-risk municipality, the total stock of SFHs alongside the number built before 1975. Fig. 17 then compares the total population to the subset of residents living in SFHs across the same municipalities. In Fig. 18, radar plots illustrate three key exposure and social-vulnerability metrics: share of women, share of residents aged 65 and over, and proportion of the population residing in SFHs, for each high-risk area. Fig. 19 depicts the structural and ownership profile of the SFH sector by showing, for each high-risk municipality, the percentage of homes built before 1975 versus the percentage of SFHs that are privately owned.

Fig. 15 highlights twelve municipalities: Stockholm, Göteborg, Malmö, Uppsala, Västerås, Linköping, Lund, Varberg, Örebro, Borlänge, Östersund, and Umeå, whose SFH sectors lie in the high SUHI risk. For example, Stockholm contains about 45,708 SFHs, of which 36,052 (79

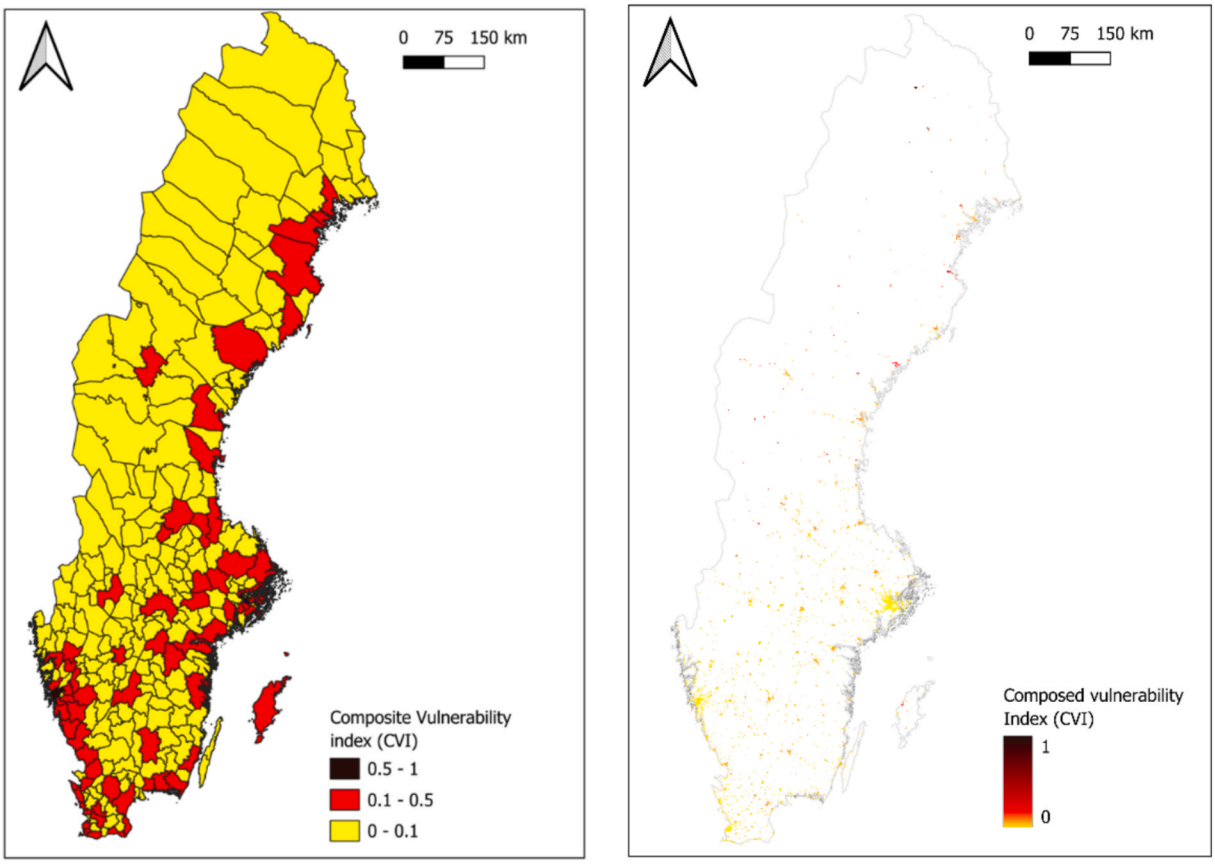


Fig. 13. SFH sector vulnerability by municipalities.

Table 8
Counties at risk by the weighting method for risk components.

County/Weighting method	Total number of deaths due to heat stress (1997–2023)	Exposure Dominant	Hazard dominant	Vulnerability dominant	Equal weights	Entropy weights
Stockholm	7	1	1	0	1	0
Västra Götaland	5	1	1	0	1	0
Skåne	4	1	1	1	1	0
Jämtland	2	1	1	0	1	1
Västmanland	2	1	1	0	1	0
Dalarna	1	1	0	0	1	0
Halland	1	1	0	0	1	0
Kalmar	1	0	1	0	1	0
Kronoberg	1	0	0	0	1	0
Uppsala	1	1	1	0	1	0
Västerbotten	1	1	1	1	1	0
Blekinge	0	0	0	0	0	0
Gävleborg	0	0	0	0	1	0
Gotland	0	0	0	0	0	0
Jönköping	0	0	1	0	1	0
Norrbotten	0	0	0	0	0	1
Örebro	0	1	1	1	1	0
Östergötland	0	1	1	0	1	0
Södermanland	0	0	1	0	1	0
Värmland	0	0	0	0	0	0
Västernorrland	0	0	0	0	1	0

Note: Cells in Red (and 1) mean the county with deaths is highlighted under risk, cells in yellow (and 1) mean the county without deaths, but it is highlighted under risk. However, cells with 0, mean the county is not under risk.

%) were built before 1975, housing 14.5 % of its 984,748 residents. Linköping has 26,290 SFHs (55 % pre-1975), accommodating 38.2 % of its population, while Östersund, despite having only 7265 SFHs, shows the highest structural and social vulnerability, with 61 % of its homes pre-1975, 22 % of residents aged 65+, and 50 % women. These figures demonstrate that high SUHI risk emerges where large numbers of homes in heated zones overlap with ageing housing stocks and more vulnerable populations, not just in the biggest cities. Table 10 presents a summary of population-related statistics and single-family housing (SFH) characteristics for municipalities identified as being at high risk from SUHI.

The analysis reveals that municipalities classified as high-risk contain approximately 191,230 single-family homes (SFHs) built

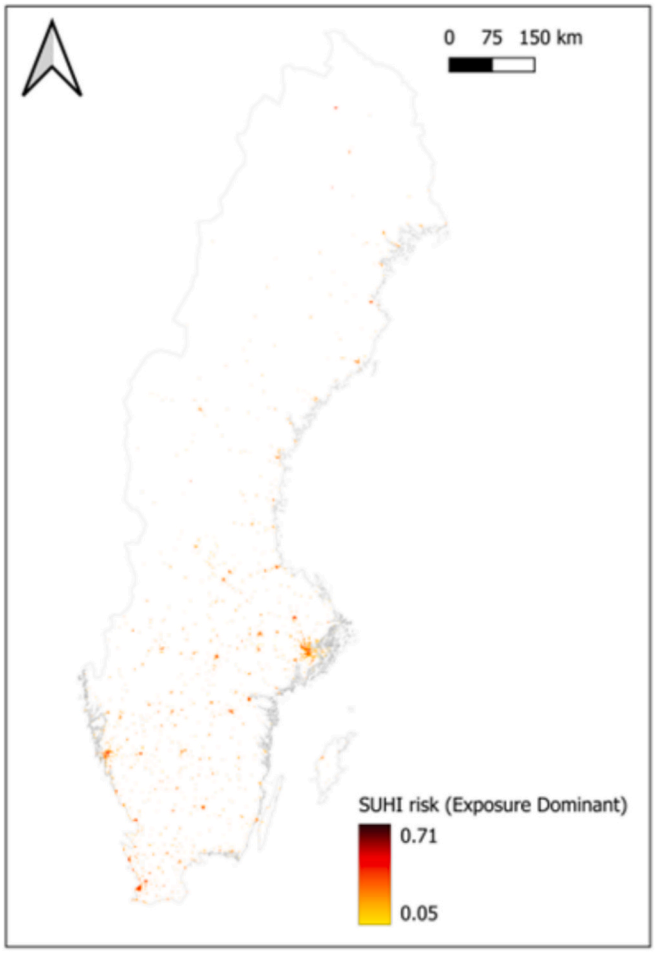


Fig. 14. SUHI risk zones for the SFH sector in Sweden. Exploring Cities and municipalities at risk to SUHI.

before 1975, accounting for around 14 % of all pre-1975 SFHs in Sweden. When medium-risk municipalities are included, this share rises to 22 % of the national total. These older buildings are particularly vulnerable to SUHI impacts in the coming decades due to their poor thermal performance and limited climate resilience. Moreover, many of these homes are occupied by elderly residents, a population group especially susceptible to heat-related health risks, underscoring the urgent need for targeted renovation and adaptation measures in these areas. The analysis assumed that the majority of the houses built before 1975 had not yet implemented climate adaptation measures such as retrofitting or air conditioning installation. The study also relied on land surface temperature (LST) data with a spatial resolution of 1 km (Figs. 4–5), which, while effective for regional assessments, limits the capture of finer-scale intra-urban temperature variations. Recognising this limitation highlights opportunities for future research to incorporate higher-resolution datasets and explore the integration of autonomous sensing technologies or IoT-based temperature sensors to enhance spatial granularity. Despite these limitations and assumptions, the study effectively maps and analyses current risks, providing a robust foundation for understanding heat vulnerability. Furthermore, the approach remains relevant for identifying high-risk areas, and dynamic mapping could certainly extend its applicability to assess risk propagation under future climatic scenarios. Ultimately, this study offers valuable insights into building adaptation strategies, presenting a scalable framework that

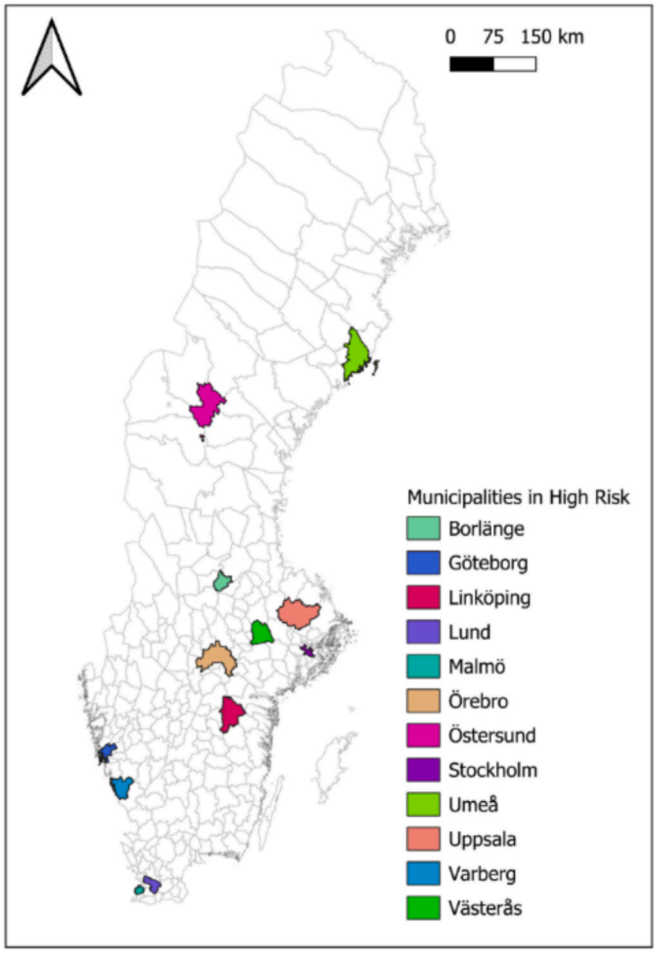


Fig. 15. Municipalities where the SFH sector is at high risk to SUHI.

Table 9
Cities where SFH sector in high risk to SUHI.

City at high risk	No. of Population by city	Municipality at high risk	County at high risk	No. of Deaths by county	Validation confidence
Stockholm	1,652,895	Stockholm	Stockholm	7	High
Göteborg	674,529	Göteborg	Västra Götaland	5	High
Malmö	339,316	Malmö	Skåne	4	High
Lund	98,308	Lund	Skåne	4	High
Västerås	131,643	Västerås	Västmanland	2	High
Östersund	53,992	Östersund	Jämtland	2	High
Uppsala	174,982	Uppsala	Uppsala	1	Moderate
Varberg	38,575	Varberg	Halland	1	Moderate
Borlänge	44,299	Borlänge	Dalarna	1	Moderate
Umeå	94,243	Umeå	Västerbotten	1	Moderate
Linköping	116,851	Linköping	Östergötland	0	Low
Örebro	128,658	Örebro	Örebro	0	Low

Table 10
Summary of population-related statistics for municipalities at high risk of SUHI.

Statistics	Total number of Population	Number of Population living in SFH	Child Population (age less than 5)	Elderly population (age 65 + yr old)	Women	SFH_built_ Befor1975 (50 yr + old)	Number of SFH	Private person owned SFH
Municipalities at High Risk	3,109,800	788,752	174,312	520,676	1,558,827	191,230	316,383	282,929
Sweden	10,521,556	4,217,228	576,367	2,147,137	5,223,232	1,365,373	2,125,269	1,925,375
Share of Sweden (%)	30	19	30	24	30	14	15	15

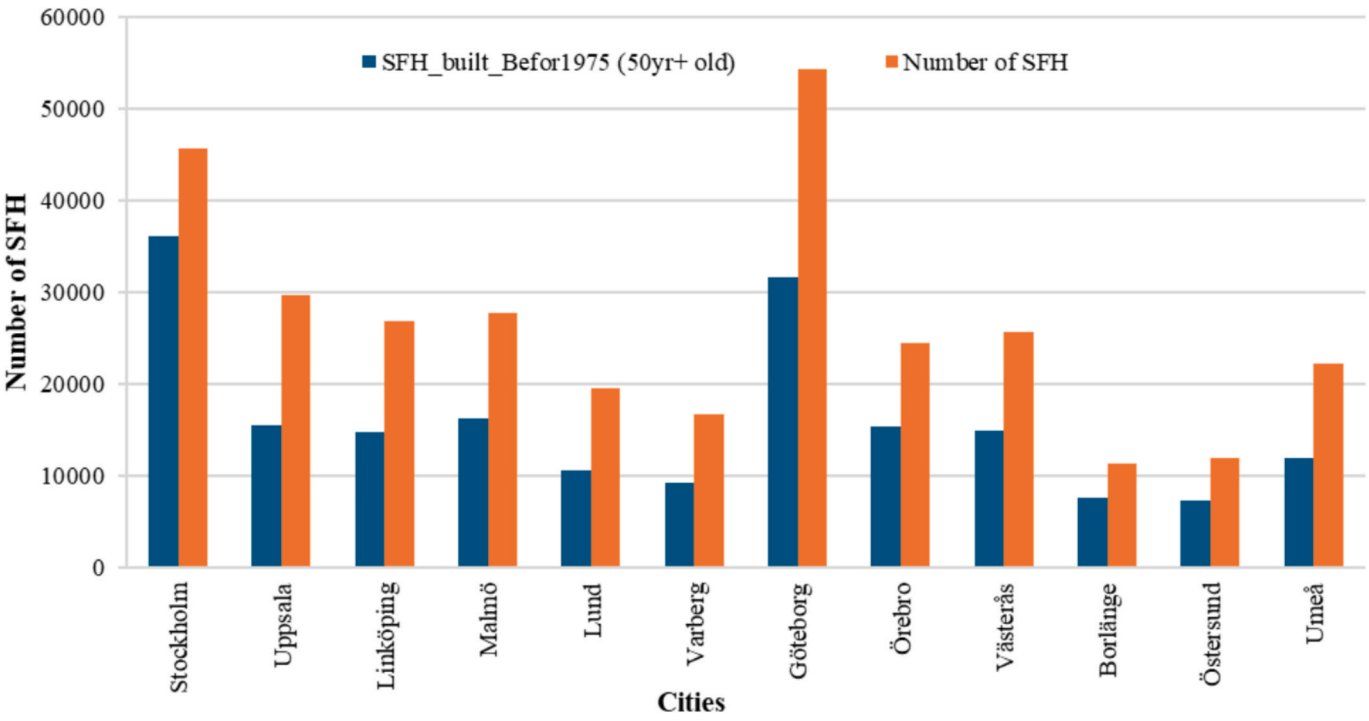


Fig. 16. Number of total SFH and SFH built before 1975 by municipalities in high-risk areas.

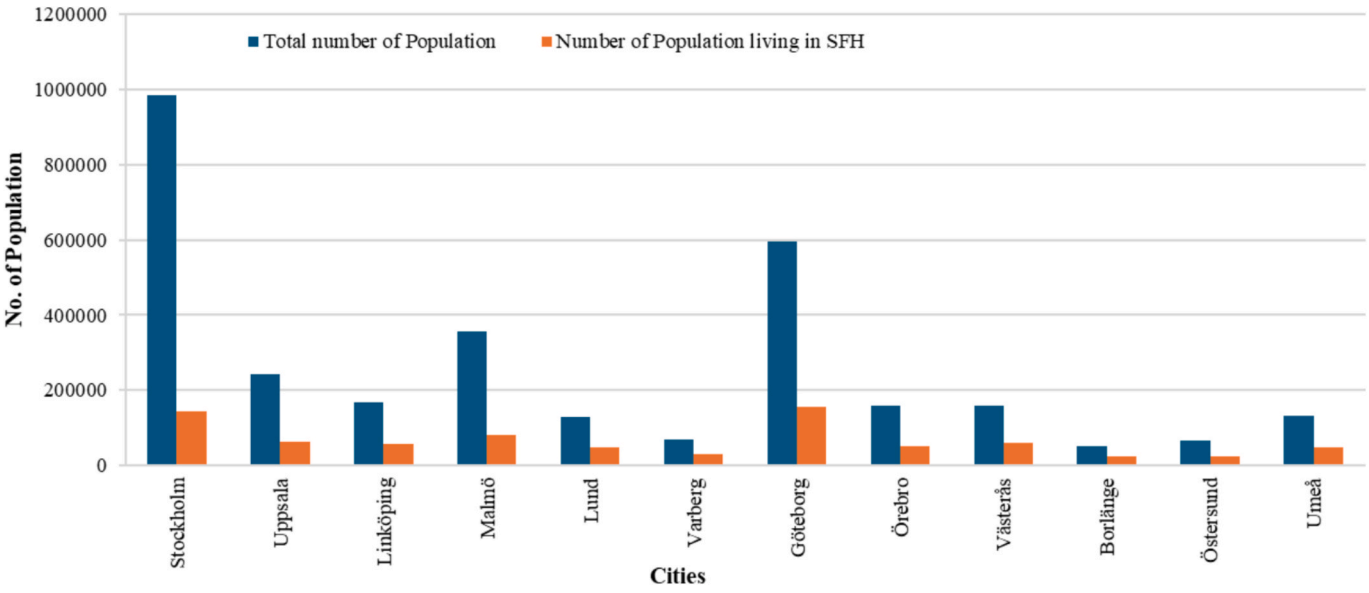


Fig. 17. Number of total SFH and SFH built before 1975 by municipalities in high-risk areas.

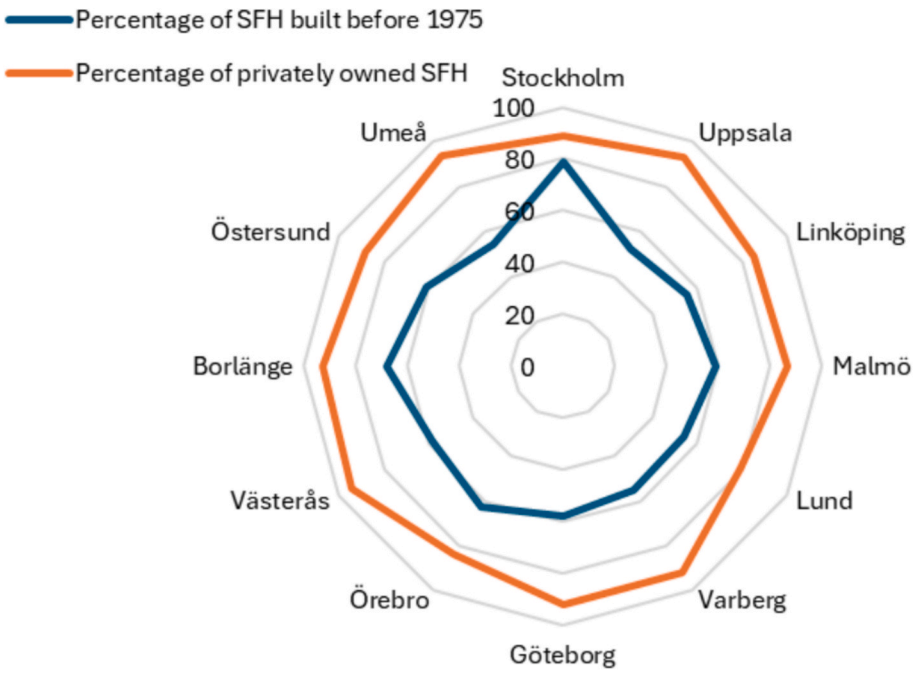


Fig. 18. Percentage of women, elderly people, and share of population living in SFH by municipalities in high-risk areas.

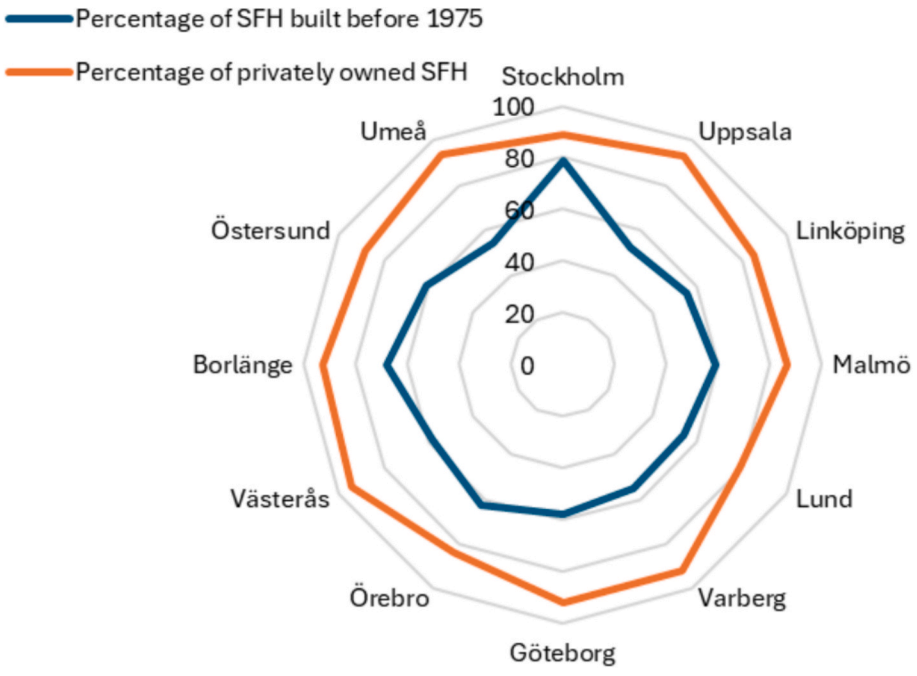


Fig. 19. Percentage of SFH built before 1975 and percentage of privately owned SFH by municipalities in high-risk areas.

can be applied beyond Sweden.

Efforts and way forward for SUHI risk management

Studies analysing Swedish municipal planning documents, surveys, and interviews reveal varied levels of progress in addressing UHI [99,100]. While some municipalities have initiated heat analyses and mitigation plans, others face barriers such as limited knowledge, financial constraints, and weak legal mandates. This fragmented approach underscores the need for coordinated municipal action to address SUHI risks through reinforced infrastructure, sustainable urban planning [101], and financial support for climate-smart renovations in vulnerable areas [102]. Measures like expanding urban green and blue infrastructure, implementing cool roofs and pavements, and using high-albedo materials, including PV modules, can significantly mitigate UHI [103]. Spatially explicit SUHI risk maps should guide the deployment of adaptive measures, particularly in neighbourhoods projected to face the highest future heat burden. Our spatial SUHI analysis identified Stockholm, Malmö, and Sundbyberg as high-risk municipalities, where SUHI intensities exceed 5 °C and over 50 % of SFHs were built before 1975. These aged homes lack adequate insulation, passive ventilation, and reflective envelope materials, making deep renovation imperative.

Reflective roofs, façades, and Building Integrated Photovoltaics (BIPV) should be prioritized in dense urban areas, such as Stockholm and Malmö, where a 10 % increase in building coverage correlates with a 3 °C rise in LST (Fig. 6b). Green roofs, vegetative shading, and urban greenery offer additional cooling benefits while improving livability and sustainability [33104]. In medium-density cities like Borlänge and Örebro, nature-based solutions such as green envelopes, linear parks, and tree-lined corridors are especially effective. Older SFHs, particularly those in coastal municipalities with low adaptation readiness, require HVAC upgrades, including zoned cooling and hybrid systems to ensure thermal comfort. Targeted subsidies, green loans, and communication strategies should motivate deep retrofits among financially capable SFH owners. One-stop-shop renovation models bundling diagnostics, customised interventions, and post-evaluation can streamline renovation action. Given Sweden's sub-target 1.2 % annual renovation rate and the estimated 500 billion SEK cost to meet the 3 % target [105,106,107], prioritising high-risk zones such as Stockholm, Malmö, and Borlänge is critical. These locally grounded strategies align with Sweden's National Climate Change Adaptation Strategy (2018), the EU Green Deal, and the Renovation Wave Initiative by promoting energy-efficient, climate-resilient buildings and reducing emissions. Integrating spatial SUHI risk analysis into multi-level governance frameworks is vital for enhancing thermal resilience and protecting the health and well-being of Sweden's most vulnerable urban populations [108].

Conclusion

This research presents a detailed evaluation of SUHI intensity in Sweden, focusing on the hazard, exposure, and vulnerability components of risk. Using a simplified approach and open-source data, the study assesses SUHI risk and building sector vulnerability, making the methodology easily replicable in other regions. Results show that southern coastal areas face the highest SUHI intensity due to elevated temperatures, dense urbanisation, population concentrations, and diverse land use patterns. The maximum average LST recorded across Sweden is 30 °C, while the minimum is 0 °C. The highest SUHI intensity, reaching 6.9 °C, occurs in the southern coastal region. Exposure is greatest in areas with high urban density, ageing pre-1975 housing stock, and a large elderly population. Most high-risk municipalities are located in the southern and southeastern parts of Sweden, where historical development patterns and urban growth have intensified heat retention. In contrast, the northwestern regions show lower SUHI risk.

Additionally, twelve high-risk municipalities contain 14 % of all SFHs built before 1975, and eighteen medium-risk municipalities contain another 8 %, together representing 22 % of Sweden's national pre-1975 SFH stock. Residents of these homes in high-risk municipalities account for 27 % of the national population living in pre-1975 SFHs, while those in medium-risk areas account for 19 %. These buildings are particularly vulnerable due to poor energy performance. Without targeted adaptation and mitigation measures—such as deep renovation—risks associated with extreme heat will continue to escalate. In these areas, increased dependence on air conditioning could further intensify SUHI effects and raise energy costs. The findings offer critical insights for policymakers, supporting informed decisions to reduce SUHI impacts across the built environment.

To address SUHI risk, an integrated approach combining nature-based solutions and targeted renovation strategies is essential. Green roofs, urban greenery [109,110], and vegetative shading can significantly reduce heat stress and enhance urban sustainability. At the same time, building retrofits should prioritise passive measures such as improved insulation, solar shading, and reflective roofing, alongside energy-efficient HVAC systems powered by renewable energy. Policy efforts should focus on promoting climate-smart renovations, especially for older SFHs in high-risk areas. Providing financial incentives for homeowners undertaking deep renovations could play a key role in increasing resilience and accelerating the transition to climate-adaptive housing. This includes motivating SFH owners in SUHI-prone areas through targeted subsidies, green loans, and clear communication of benefits such as improved comfort, reduced energy costs, and climate resilience. The growing use of one-stop shops, offering integrated support from assessment to implementation, further simplifies the renovation process. A coordinated effort involving municipalities, financial institutions, and renovation stakeholders is crucial to minimising risks and ensuring effective adaptation.

This paper provides a strong foundation by mapping SUHI risk and identifying high-risk municipalities, offering actionable insights for authorities to prioritise and guide intervention efforts more effectively.

CRediT authorship contribution statement

Charafeddine Mokhtara: Writing – review & editing, Writing – original draft, Visualization, Methodology, Formal analysis, Data curation, Conceptualization. **Shashwat Sinha:** Writing – review & editing, Visualization, Validation, Methodology, Conceptualization. **Ashmin Aryal:** Writing – review & editing, Writing – original draft, Visualization, Methodology, Conceptualization. **Brijesh Mainali:** Writing – review & editing, Supervision, Methodology. **Krushna Mahapatra:** Writing – review & editing, Conceptualization.

Declaration of competing interest

The authors declare that they have no known competing financial interests or personal relationships that could have appeared to influence the work reported in this paper.

Acknowledgements

This work was supported by the Swedish Research Council for Sustainable Development (FORMAS) (Grant No. 2021-02389), under the project: "How prepared are Swedish detached houses to adapt to climate change?"

Data availability

Data will be made available on request.

References

[1] IPCC, Climate Change 2023: Synthesis Report, 2023. doi: doi:10.59327/IPCC/AR6-9789291691647.
[2] UNCTAD. Handbook of Statistics 2023. United Nations Publication; 2023.
[3] Abdulrasheed M, MacKenzie AR, Whyatt JD, Chapman L. Allometric scaling of thermal infrared emitted from UK cities and its relation to urban form. City Environ Interact 2020;5. https://doi.org/10.1016/j.cacint.2020.100037.
[4] Tarpani E, Bitossi L, Cureau R, Pigliautile I, Biscarini C, Pisello AL. Revitalizing tactical urban parks (TUPs) through environmental monitoring and participatory approaches for urban overheating mitigation. City Environ Interact 2024;24. https://doi.org/10.1016/j.cacint.2024.100164.
[5] Taha H. Urban climates and heat islands: albedo, evapotranspiration, and anthropogenic heat. Energ Build 1997;25:99–103.
[6] Oke TR. The energetic basis of the urban heat island. Quart J R Met Soc 1982;108:551.
[7] Kolokotsa D, Lilli K, Gobakis K, Mavrigiannaki A, Haddad S, Garshasbi S, et al. Analyzing the impact of urban planning and building typologies in urban heat island mitigation. Buildings 2022;12. https://doi.org/10.3390/buildings12050537.
[8] Wei Y, Lemoy R, Caruso G. The effect of population size on urban heat island and NO2 air pollution: review and meta-analysis. City Environ Interact 2024;24. https://doi.org/10.1016/j.cacint.2024.100161.
[9] Cheval S, Dumitrescu A, Irașoc A, Paraschiv MG, Perry M, Ghent D. MODIS-based climatology of the Surface Urban Heat Island at country scale (Romania). Urban Clim 2022;41:101056. https://doi.org/10.1016/j.uclim.2021.101056.
[10] Zhou D, Zhao S, Liu S, Zhang L, Zhu C. Surface urban heat island in China's 32 major cities: Spatial patterns and drivers. Remote Sens Environ 2014;152:51–61. https://doi.org/10.1016/j.rse.2014.05.017.
[11] Schwaab J. Sprawl or compactness? how urban form influences urban surface temperatures in Europe. City Environ Interact 2022;16. https://doi.org/10.1016/j.cacint.2022.100091.

[12] Santamouris M, Cartalis C, Synnefa A, Kolokotsa D. On the impact of urban heat island and global warming on the power demand and electricity consumption of buildings – a review. Energ Build 2015;98:119–24. https://doi.org/10.1016/j.enbuild.2014.09.052.
[13] Ranagalage M, Estoque RC, Zhang X, Murayama Y. Spatial changes of urban heat island formation in the Colombo District, Sri Lanka: implications for sustainability planning. Sustainability (Switzerland) 2018;10. https://doi.org/10.3390/su10051367.
[14] Diem PK, Nguyen CT, Diem NK, Diep NTH, Thao PTB, Hong TG, et al. Remote sensing for urban heat island research: progress, current issues, and perspectives. Remote Sens Appl 2024;33. https://doi.org/10.1016/j.rsase.2023.101081.
[15] Zhou D, Xiao J, Bonafoni S, Berger C, Deilami K, Zhou Y, et al. Satellite remote sensing of surface urban heat islands: progress, challenges, and perspectives. Remote Sens (Basel) 2019;11. https://doi.org/10.3390/rs11010048.
[16] Steensen BM, Marelle L, Hodnebrog, Myhre G. Future urban heat island influence on precipitation. Clim Dyn 2022;58:3393–403. https://doi.org/10.1007/s00382-021-06105-z.
[17] Drebs A, Suomi J, Mäkelä A. Urban heat island research at high latitudes — utilising Finland as an example. Boreal Environ Res 2023;28:81–96.
[18] Drebs A, Suomi J. Antti Mäkelä, Urban heat island research at high latitudes-utilising Finland as an example. Boreal Environ Res 2023;28:81–96. https://www.researchgate.net/publication/370025041.
[19] SCB, Statistics Sweden, Https://Www.Scb.Se/ (2023). https://www.scb.se/ (accessed October 15, 2023).
[20] Hall T, Vidén S. The million homes programme: a review of the great swedish planning project. Plan Perspect 2005;20:301–28. https://doi.org/10.1080/02665430500130233.
[21] Brunnström P, Håkansson PG, Uppenberg C. Migration and housing regimes in Sweden 1739–1982. Scand J Hist 2021;46:353–82. https://doi.org/10.1080/03468755.2020.1843532.
[22] Sula M, K. Mahapatra, B. Mainali, Addressing housing shortage through energy and space-efficient retrofitting: The case study of a Swedish Single-Family house, in: IOP Conf Ser Earth Environ Sci, Institute of Physics, 2022: p. 40DUMMY. doi: 10.1088/1755-1315/1085/1/012038.
[23] Pardalis G, Mahapatra K, Mainali B. Comparing public- and private-driven one-stop-shops for energy renovations of residential buildings in Europe. J Clean Prod 2022;365. https://doi.org/10.1016/j.jclepro.2022.132683.
[24] Swedish Meteorological and Hydrological Institute, Ordinance (2018:1428) on climate adaptation work on the part of government agencies, 2018. https://www.smhi.se/polopoly_fs/1.168055!/ordinance.pdf (accessed October 1, 2024).
[25] Mokhtara C, Negrou B, Settou N, Bouferrouk A, Yao Y. Optimal design of grid-connected rooftop PV systems: an overview and a new approach with application to educational buildings in arid climates. Sustainable Energy Technol Assess 2021;47. https://doi.org/10.1016/j.seta.2021.101468.
[26] Othman HAS, Alshboul AA. The role of urban morphology on outdoor thermal comfort: the case of Al-Sharq City – Az Zarqa. Urban Clim 2020;34. https://doi.org/10.1016/j.uclim.2020.100706.
[27] Kotharkar R, Bagade A, Singh PR. A systematic approach for urban heat island mitigation strategies in critical local climate zones of an Indian city. Urban Clim 2020;34. https://doi.org/10.1016/j.uclim.2020.100701.
[28] Li F, Sun W, Yang G, Weng Q. Investigating spatiotemporal patterns of surface Urban heat islands in the Hangzhou Metropolitan area, China, 2000-2015. Remote Sens (Basel) 2019;11. https://doi.org/10.3390/rs11131553.
[29] Vinayak B, Lee HS, Gedam S, Latha R. Impacts of future urbanization on urban microclimate and thermal comfort over the Mumbai metropolitan region, India. Sustain Cities Soc 2022;79. https://doi.org/10.1016/j.scs.2022.103703.
[30] Stone B, Mallen E, Rajput M, Broadbent A, Krayenhoff ES, Augenbroe G, et al. Climate change and infrastructure risk: Indoor heat exposure during a concurrent heat wave and blackout event in Phoenix, Arizona. Urban Clim 2021;36. https://doi.org/10.1016/j.uclim.2021.100787.
[31] Zhou SQ, Yu ZW, Ma WY, Yao XH, Xiong JQ, Ma WJ, et al. Vertical canopy structure dominates cooling and thermal comfort of urban pocket parks during hot summer days. Landsc Urban Plan 2025;254. https://doi.org/10.1016/j.landurbplan.2024.105242.
[32] Kabisch N, van den Bosch M, Lafortezza R. The health benefits of nature-based solutions to urbanization challenges for children and the elderly – a systematic review. Environ Res 2017;159:362–73. https://doi.org/10.1016/j.envres.2017.08.004.
[33] Li Y, Svenning JC, Zhou W, Zhu K, Abrams JF, Lenton TM, et al. Green spaces provide substantial but unequal urban cooling globally. Nat Commun 2024;15. https://doi.org/10.1038/s41467-024-51355-0.
[34] Zhang M, Yiğit İ, Adigüzel F, Hu C, Chen E, Siyavuş AE, et al. Impact of urban surfaces on microclimatic conditions and thermal comfort in Burdur, Türkiye. Atmosphere (Basel) 2024;15. https://doi.org/10.3390/atmos15111375.
[35] Mughal MO, Kubilay A, Fatichi S, Meili N, Carmeliet J, Edwards P, et al. Detailed investigation of vegetation effects on microclimate by means of computational fluid dynamics (CFD) in a tropical urban environment. Urban Clim 2021;39. https://doi.org/10.1016/j.uclim.2021.100939.
[36] Xue F, Gou Z, Lau SSY. Green open space in high-dense asian cities: Site configurations, microclimates and users' perceptions. Sustain Cities Soc 2017;34:114–25. https://doi.org/10.1016/j.scs.2017.06.014.
[37] Wu B, Zhang Y, Wang Y, He Y, Wang J, Wu Y, et al. Mitigation of urban heat island in China (2000–2020) through vegetation-induced cooling. Sustain Cities Soc 2024;112. https://doi.org/10.1016/j.scs.2024.105599.
[38] Zhang M, Tan S, Liang J, Zhang C, Chen E. Predicting the impacts of urban development on urban thermal environment using machine learning algorithms in Nanjing, China. J Environ Manage 2024;356. https://doi.org/10.1016/j.jenvman.2024.120560.
[39] Hu C, Zhang M, Huang G, Li Z, Sun Y, Zhao J. Tracking the impact of the land cover change on the spatial-temporal distribution of the thermal comfort: Insights from the Qinhuai River Basin, China. Sustain Cities Soc 2024;116. https://doi.org/10.1016/j.scs.2024.105916.
[40] Zhao J, Hu C, Li Z, Zhang M, Fan H, Li K, et al. Investigating the quantitative impact of the vegetation indices on the urban thermal comfort based on machine learning: a case study of the Qinhuai River Basin, China. Sustain Cities Soc 2025;125. https://doi.org/10.1016/j.scs.2025.106357.
[41] Mohammad Harmay NS, Kim D, Choi M. Urban heat island associated with land use/land cover and climate variations in Melbourne, Australia. Sustain Cities Soc 2021;69. https://doi.org/10.1016/j.scs.2021.102861.
[42] Ullah N, Siddique MA, Ding M, Grigoryan S, Khan IA, Kang Z, et al. The impact of urbanization on urban heat island: predictive approach using google earth engine and CA-Markov modelling (2005–2050) of Tianjin City, China. Int J Environ Res Public Health 2023;20. https://doi.org/10.3390/ijerph20032642.
[43] Ngarambe J, Oh JW, Su MA, Santamouris M, Yun GY. Influences of wind speed, sky conditions, land use and land cover characteristics on the magnitude of the urban heat island in Seoul: an exploratory analysis. Sustain Cities Soc 2021;71. https://doi.org/10.1016/j.scs.2021.102953.
[44] Shi Y, Zhang Y. Urban morphological indicators of urban heat and moisture islands under various sky conditions in a humid subtropical region. Build Environ 2022;214. https://doi.org/10.1016/j.buildenv.2022.108906.
[45] Al-Obaidi I, Rayburg S, Półrolniczak M, Neave M. Assessing the impact of wind conditions on urban heat islands in large Australian Cities. J Ecol Eng 2021;22:1–15. https://doi.org/10.12911/22998993/142967.
[46] Yang B, Meng F, Ke X, Ma C. The impact analysis of water body landscape pattern on urban heat Island: a case study of Wuhan city. Adv Meteorol 2015;2015. https://doi.org/10.1155/2015/416728.
[47] Wong PPY, Lai PC, Low CT, Chen S, Hart M. The impact of environmental and human factors on urban heat and microclimate variability. Build Environ 2016;95:199–208. https://doi.org/10.1016/j.buildenv.2015.09.024.
[48] Fan C, Myint SW, Kaplan S, Middel A, Zheng B, Rahman A, et al. Understanding the impact of urbanization on surface urban heat Islands-a longitudinal analysis of the oasis effect in subtropical desert cities. Remote Sens (Basel) 2017;9. https://doi.org/10.3390/rs9070672.
[49] Ejiagha IR, Ahmed MR, Dewan A, Gupta A, Rangelova E, Hassan QK. Urban Warming of the two Most Populated Cities in the Canadian Province of Alberta, and its Influencing Factors. Sensors 2022;22. https://doi.org/10.3390/s22082894.
[50] Koko AF, Yue W, Abubakar GA, Alabsi AAN, Hamed R. Spatiotemporal influence of land use/land cover change dynamics on surface urban heat island: a case study of abuja metropolis, nigeria. ISPRS Int J Geoinf 2021;10. https://doi.org/10.3390/ijgi10050272.
[51] Dewan A, Kiselev G, Botje D. Diurnal and seasonal trends and associated determinants of surface urban heat islands in large Bangladesh cities. Appl Geogr 2021;135. https://doi.org/10.1016/j.apgeog.2021.102533.
[52] Santamouris M. Analyzing the heat island magnitude and characteristics in one hundred asian and Australian cities and regions. Sci Total Environ 2015;512–513:582–98. https://doi.org/10.1016/j.scitotenv.2015.01.060.
[53] Huang X, Wang Y. Investigating the effects of 3D urban morphology on the surface urban heat island effect in urban functional zones by using high-resolution remote sensing data: a case study of Wuhan, Central China. ISPRS J Photogramm Remote Sens 2019;152:119–31. https://doi.org/10.1016/j.isprsjprs.2019.04.010.
[54] Chen J, Wang K, Du P, Zang Y, Zhang P, Xia J, et al. Quantifying the main and interactive effects of the dominant factors on the diurnal cycles of land surface temperature in typical urban functional zones. Sustain Cities Soc 2024;114. https://doi.org/10.1016/j.scs.2024.105727.
[55] J. Li, J. Wang, N.H. Wong, Urban Micro-climate Research in High Density Cities: Case Study in Nanjing, in: Procedia Eng, Elsevier Ltd, 2016: pp. 88–99. doi: 10.1016/j.proeng.2016.10.011.
[56] János U. Intra-urban relationship between surface geometry and urban heat island: review and new approach. Clim Res 2004;27. 253–264. www.int-res.com.
[57] Agathangelidis I, Cartalis C, Santamouris M. Urban morphological controls on surface thermal dynamics: a comparative assessment of major european cities with a focus on Athens, Greece. Climate 2020;8:1–33. https://doi.org/10.3390/cli8110131.
[58] Zhou B, Rybski D, Kropp JP. The role of city size and urban form in the surface urban heat island. Sci Rep 2017;7. https://doi.org/10.1038/s41598-017-04242-2.
[59] Kim J, Lee DK, Brown RD, Kim S, Kim JH, Sung S. The effect of extremely low sky view factor on land surface temperatures in urban residential areas. Sustain Cities Soc 2022;80. https://doi.org/10.1016/j.scs.2022.103799.
[60] Choudhury D, Das K, Das A. Assessment of land use land cover changes and its impact on variations of land surface temperature in Asansol-Durgapur Development Region. Egypt J Remote Sens Space Sci 2019;22:203–18. https://doi.org/10.1016/j.ejrs.2018.05.004.
[61] Sahana M, Ahmed R, Sajjad H. Analyzing land surface temperature distribution in response to land use/land cover change using split window algorithm and spectral radiance model in Sundarban Biosphere Reserve, India. Model Earth Syst Environ 2016;2. https://doi.org/10.1007/s40808-016-0135-5.
[62] Faragallah RN, Ragheb RA. Evaluation of thermal comfort and urban heat island through cool paving materials using ENVI-Met. Ain Shams Eng J 2022;13. https://doi.org/10.1016/j.asej.2021.10.004.

[63] Wang A, Dai Y, Zhang M, Chen E. Exploring the cooling intensity of green cover on urban heat island: a case study of nine main urban districts in Chongqing. Sustain Cities Soc 2025;124. https://doi.org/10.1016/j.scs.2025.106299.
[64] Hoffmann P, Heinke SchlüNzen K. Weather pattern classification to represent the urban heat island in present and future climate. J Appl Meteorol Climatol 2013; 52:2699–714. https://doi.org/10.1175/JAMC-D-12-065.1.
[65] McCarthy MP, Best MJ, Betts RA. Climate change in cities due to global warming and urban effects. Geophys Res Lett 2010;37. https://doi.org/10.1029/2010GL042845.
[66] Oleson KW, Monaghan A, Wilhelmi O, Barlage M, Brunsell N, Feddema J, et al. Interactions between urbanization, heat stress, and climate change. Clim Change 2015;129:525–41. https://doi.org/10.1007/s10584-013-0936-8.
[67] Kamal A, Mahfouz A, Sezer N, Hassan IG, Wang LL, Rahman MA. Investigation of urban heat island and climate change and their combined impact on building cooling demand in the hot and humid climate of Qatar. Urban Clim 2023;52. https://doi.org/10.1016/j.uclim.2023.101704.
[68] Zhu H, Wang A, Wang P, Hu C, Zhang M. Spatiotemporal dynamics and response of land surface temperature and kernel normalized difference vegetation index in Yangtze River Economic Belt, China: multi-method analysis. Land (Basel) 2025; 14. https://doi.org/10.3390/land14030598.
[69] Chapman S, Watson JEM, Salazar A, Thatcher M, McAlpine CA. The impact of urbanization and climate change on urban temperatures: a systematic review. Landsc Ecol 2017;32:1921–35. https://doi.org/10.1007/s10980-017-0561-4.
[70] Monteiro FF, Gonçalves WA, Andrade L de MB, Villavicencio LMM, dos Santos Silva CM. Assessment of Urban Heat Islands in Brazil based on MODIS remote sensing data. Urban Clim 2021;35. https://doi.org/10.1016/j.uclim.2020.100726.
[71] Gaur A, Eichenbaum MK, Simonovic SP. Analysis and modelling of surface Urban Heat Island in 20 Canadian cities under climate and land-cover change. J Environ Manage 2018;206:145–57. https://doi.org/10.1016/j.jenvman.2017.10.002.
[72] Liu Y, Li Q, Yang L, Mu K, Zhang M, Liu J. Urban heat island effects of various urban morphologies under regional climate conditions. Sci Total Environ 2020; 743. https://doi.org/10.1016/j.scitotenv.2020.140589.
[73] Liu Y, Fang X, Xu Y, Zhang S, Luan Q. Assessment of surface urban heat island across China's three main urban agglomerations. Theor Appl Climatol 2018;133: 473–88. https://doi.org/10.1007/s00704-017-2197-3.
[74] Hellings A, Rienow A. Mapping land surface temperature developments in functional urban areas across europe. Remote Sens (Basel) 2021;13. https://doi.org/10.3390/rs13112111.
[75] Possega M, Aragão L, Ruggieri P, Santo MA, Di Sabatino S. Observational evidence of intensified nocturnal urban heat island during heatwaves in European cities. Environ Res Lett 2022;17. https://doi.org/10.1088/1748-9326/aca3ba.
[76] Raj S, Paul SK, Chakraborty A, Kuttippurath J. Anthropogenic forcing exacerbating the urban heat islands in India. J Environ Manage 2020;257. https://doi.org/10.1016/j.jenvman.2019.110006.
[77] Morabito M, Crisci A, Guerri G, Messeri A, Congedo L, Munafò M. Surface urban heat islands in italian metropolitan cities: tree cover and impervious surface influences. Sci Total Environ 2021;751. https://doi.org/10.1016/j.scitotenv.2020.142334.
[78] Cheval S, Dumitrescu A, Irașoc A, Paraschiv MG, Perry M, Ghent D. MODIS-based climatology of the Surface Urban Heat Island at country scale (Romania). Urban Clim 2022;41. https://doi.org/10.1016/j.uclim.2021.101056.
[79] Miles V, Esau I. Surface urban heat islands in 57 cities across different climates in northern Fennoscandia. Urban Clim 2020;31. https://doi.org/10.1016/j.uclim.2019.100575.
[80] Fu P, Weng Q. Variability in annual temperature cycle in the urban areas of the United States as revealed by MODIS imagery. ISPRS J Photogramm Remote Sens 2018;146:65–73. https://doi.org/10.1016/j.isprsjprs.2018.09.003.
[81] Imhoff ML, Zhang P, Wolfe RE, Bounoua L. Remote sensing of the urban heat island effect across biomes in the continental USA. Remote Sens Environ 2010; 114:504–13. https://doi.org/10.1016/j.rse.2009.10.008.
[82] IPCC, IPCC's Fifth Assessment Report (AR5), Report (2014). https://www.ipcc.ch/report/ar5/syr/ (accessed December 1, 2023).
[83] IPCC, Climate Change 2014 Impacts, Adaptation, and Vulnerability Part A: Global and Sectoral Aspects, 2014.
[84] Climate change knowledge portal, Climate change knowledge portal, Https://Climateknowledgeportal.Worldbank.Org/Country/Sweden (2024). https://climateknowledgeportal.worldbank.org/country/sweden (accessed July 16, 2024).
[85] Swedish Meteorological and Hydrological Institute (SMHI), Climate indicator, (2023). https://www.smhi.se/klimat/klimatet-da-och-nu/klimatindikatorer/klimatindikator-temperatur-1.2430 (accessed January 2, 2025).
[86] TABULA, TABULA WebTool, Https://Webtool.Building-Typology.Eu/#bm (2024). https://webtool.building-typology.eu/#bm (accessed March 16, 2024).
[87] OSM, Open street map, Https://Www.Openstreetmap.Org/#map=4/62.99/17.64 (2024). https://www.openstreetmap.org/#map=4/62.99/17.64 (accessed March 16, 2024).
[88] Zargari M, Mofidi A, Entezari A, Baaghideh M. Climatic comparison of surface urban heat island using satellite remote sensing in Tehran and suburbs. Sci Rep 2024;14:1–23. https://doi.org/10.1038/s41598-023-50757-2.
[89] Verichev K, Salazar-Concha C, Díaz-López C, Carpio M. The influence of the urban heat island effect on the energy performance of residential buildings in a city with an oceanic climate during the summer period: case of Valdivia, Chile. Sustain Cities Soc 2023;97. https://doi.org/10.1016/j.scs.2023.104766.
[90] Li F, Yigitcanlar T, Nepal M, Thanh KN, Dur F. Understanding urban heat vulnerability assessment methods: a PRISMA review. Energies (Basel) 2022;15: 1–34. https://doi.org/10.3390/en15196998.
[91] Wu RMX, Zhang Z, Yan W, Fan J, Gou J, Liu B, et al. A comparative analysis of the principal component analysis and entropy weight methods to establish the indexing measurement. PLoS One 2022;17. https://doi.org/10.1371/journal.pone.0262261.
[92] Taylor J, Simpson CH, Vanhatalo J, Sohail H, Brousse O, Heaviside C. Analysing cold-climate urban heat islands using personal weather station data. Build Cities 2025;6:182–200. https://doi.org/10.5334/bc.528.
[93] Martin P, Baudouin Y, Gachon P. An alternative method to characterize the surface urban heat island. Int J Biometeorol 2015;59:849–61. https://doi.org/10.1007/s00484-014-0902-9.
[94] Weng Q, Lu D, Schubring J. Estimation of land surface temperature-vegetation abundance relationship for urban heat island studies. Remote Sens Environ 2004; 89:467–83. https://doi.org/10.1016/j.rse.2003.11.005.
[95] Yao X, Jin S, Zhao Z, Sun R, Wang C, Yu Z. A novel integrated socio-ecological-economic index for assessing heat health risk. Ecol Ind 2024;169. https://doi.org/10.1016/j.ecolind.2024.112840.
[96] Morabito M, Crisci A, Moriondo M, Profili F, Francesconi P, Trombi G, et al. Air temperature-related human health outcomes: current impact and estimations of future risks in Central Italy. Sci Total Environ 2012;441:28–40. https://doi.org/10.1016/j.scitotenv.2012.09.056.
[97] Morabito M, Crisci A, Gioli B, Gualtieri G, Toscano P, Di Stefano V, et al. Urban-hazard risk analysis: mapping of heat-related risks in the elderly in major Italian cities. PLoS One 2015;10. https://doi.org/10.1371/journal.pone.0127277.
[98] Schneider R. Extreme events require new forms of financial collaboration to become more resilient. Springer; 2023. 10.1007/s10669-023-09944-9.
[99] Kindberg E. Climate adaptation to urban heat: a study of how Swedish municipalities with larger cities are adapting to warmer temperatures through urban planning. Linköping University; 2023.
[100] Håkansson M. Adapt to climate change or pay the price two Swedish municipalities' approaches to climate adaptation in urban planning. Linköping University; 2023.
[101] Gómez-Villarino MT, Gómez Villarino M, Ruiz-Garcia L. Implementation of urban green infrastructures in peri-urban areas: a case study of climate change mitigation in madrid. Agronomy 2021;11. https://doi.org/10.3390/agronomy11010031.
[102] Bertoldi P, Economidou M, Palermo V, Boza-Kiss B, Todeschi V. How to finance energy renovation of residential buildings: review of current and emerging financing instruments in the EU. Wiley Interdiscip Rev: Energy Environ 2021;10. https://doi.org/10.1002/wene.384.
[103] Sharifi A, Yamagata Y. Roof ponds as passive heating and cooling systems: a systematic review. Appl Energy 2015;160:336–57. https://doi.org/10.1016/j.apenergy.2015.09.061.
[104] Zhou SQ, Yu ZW, Ben Wu W, Yang WJ, Zhang YJ, Hao YY, et al. Quantifying cumulative cooling threshold of greenspaces using a newly developed 3D model across global cities. Remote Sens Environ 2025;328. https://doi.org/10.1016/j.rse.2025.114867.
[105] Sula M, Mahapatra K, Mainali B. Unveiling the perspectives of Swedish homeowners on embracing space sufficiency within the context of energy renovation. Energ Build 2025;328. https://doi.org/10.1016/j.enbuild.2024.114997.
[106] Khadra A, Akander J, Zhang X, Myhren JA. Assessing the economic and environmental dimensions of large-scale energy-efficient renovation decisions in district-heated multifamily buildings from both the building and urban energy system perspectives. Energies (Basel) 2025;18. https://doi.org/10.3390/en18030513.
[107] Under Miljonprogrammet Byggdes en Miljon Bostäder. Boverket, (n.d.). https://www.boverket.se/sv/samhallsplanering/stadsutveckling/miljonprogrammet/ (accessed February 22, 2025).
[108] Cheval S, Amihăesei VA, Chitu Z, Dumitrescu A, Falcescu V, Irașoc A, et al. A systematic review of urban heat island and heat waves research (1991–2022). Clim Risk Manag 2024;44. https://doi.org/10.1016/j.crm.2024.100603.
[109] Yu Z, Li S, Yang W, Chen J, Rahman MA, Wang C, et al. Enhancing climate-driven urban tree cooling with targeted nonclimatic interventions. Environ Sci Technol 2025;59:9082–92. https://doi.org/10.1021/acs.est.4c14275.
[110] Yu Z, Chen J, Chen J, Zhan W, Wang C, Ma W, et al. Enhanced observations from an optimized soil-canopy-photosynthesis and energy flux model revealed evapotranspiration-shading cooling dynamics of urban vegetation during extreme heat. Remote Sens Environ 2024;305. https://doi.org/10.1016/j.rse.2024.114098.